Capacity of Skirted Foundations in Sand-over-Clay under Combined V-H-M Loading

Xinjun Zou[1], Yuxia Hu[2], Muhammad Shazzad Hossain[3] and Mi Zhou[4]

[1]Associate Professor (PhD), College of Civil Engineering, Hunan University, Changsha 410082, P. R. China; Visiting Research Fellow, School of Civil and Resource Engineering, The University of Western Australia, 35 Stirling Highway, Crawley, WA 6009, Tel: +61 (0)8 6488 8182, Fax: +61 (0)8 6488 1018; Email: xjzouhd@hnu.edu.cn

[2]Professor (PhD, MIEAust), School of Civil, Environmental and Mining Engineering, The University of Western Australia, 35 Stirling Highway, Crawley, WA 6009, Tel: +61 8 6488 8182, Fax: +61 8 6488 1018, Email: yuxia.hu@uwa.edu.au

[3]Senior Research Fellow (BEng, MEng, PhD, MIEAust), Centre for Offshore Foundation Systems (COFS), The University of Western Australia, 35 Stirling Highway, Crawley, WA 6009, Tel: +61 8 6488 7358, Fax: +61 8 6488 1044, Email: muhammad.hossain@uwa.edu.au

[4]Corresponding author, Associate professor (PhD), State Key laboratory of Subtropical Building Science, South China Institute of Geotechnical Engineering. State, South China University of Technology, 381 Wushan Road, Guangzhou 510640 China, Tel: +86 20 87111029, Fax: +86 20 87111029; Email: michaelmizhou@163.com

- Number of Words: 4077 (text only)
- Number of Tables: 03
- Number of Figures: 17

Capacity of Skirted Foundations in Sand-over-Clay under Combined V-H-M Loading

Abstract

Circular skirted foundations are used widely in the offshore oil and gas industry and renewable energy industry to support subsea infrastructure and founding turbines. The foundations are subjected to combined vertical-horizontal-moment (*V*-*H*-*M*) loadings during operation. This paper describes an extensive investigation of the response of installed circular skirted foundations under operational loadings in sand-over-clay. The overarching aim was to examine the influence of the presence of a sand layer on the combined load capacity. A detailed parametric study was undertaken through small strain finite element analyses, varying the thickness of the sand layer, embedment depth of the foundation (or skirt length), and level of vertical load mobilization.

The effect of the surface sand layer was profound for thicker sand layer of $T_s/D > 0.2$. Normalized failure envelopes were presented in *v*-*h*, *v*-*m* and *h*-*m* spaces. The FE results on the former two spaces showed unique trend, but not on the latter. New approximating expressions for describing the failure envelopes as a function of the sand layer thickness ratio, skirt length ratio and vertical load mobilization level were proposed.

KEYWORDS: bearing capacity; failure; footings/foundations; numerical modelling; offshore engineering; sands

NOTATION

A	foundation base area at skirt tip level
a	fitting constant
c	cohesion
D	foundation diameter
d	skirt length
E	Young's modulus
H	horizontal load
H_{ult}	uniaxial (pure) horizontal capacity
h	$h = H/H_{ult}$
h_0	dimensionless uniaxial horizontal capacity, $h_0 = H_{ult}/As_{u0}$
$h_{0,Ts=0}$	h_0 in absence of sand layer
k	clay strength gradient
M	moment
M_{max}	maximum moment
M_{ult}	uniaxial moment capacity
M^*	moment capacity at $h = 0$
m	$m = M/M_{ult}$
m^*	$m^* = M/M^*$

64	m_0	dimensionless uniaxial moment capacity, $m_0 = M_{ult}/As_{u0}$
65	$m_{0,Ts=0}$	m_0 in absence of sand layer
66	m_{max}	$m_{max} = M_{max}/M_{ult}$
67	N_c, N_γ	dimensionless bearing capacity factors
68	s_u	undrained shear strength
69	s_{u0}	undrained shear strength at skirt tip level
70	s_{umc}	undrained shear strength at sand-clay interface
71	t	skirt wall thickness
72	T_s	surface sand layer thickness
73	u	horizontal displacement
74	V	vertical load
75	V_{ult}	uniaxial vertical capacity
76	v	$v = V/V_{ult}$
77	v_0	dimensionless uniaxial vertical capacity, $v_0 = V_{ult}/As_{u0}$
78	$v_{0,Ts=0}$	dimensionless uniaxial vertical capacity, $v_0 = V_{ult}/As_{u0}$ for $T_s = 0$
79	w	vertical displacement
80	z	depth below soil surface
81	θ	rotation angle
82	α	fitting parameter

β	fitting parameter
γ'_c	effective unit weight of clay
γ'_s	effective unit weight of sand
ϕ	friction angle
ψ	dilation angle
ν	Poisson's ratio
κ_c	clay strength non-homogeneity, kD/s_{umc}

1 INTRODUCTION

Circular skirted foundations (colloquially known as ‘bucket foundations’ or ‘suction caissons’) are used widely in the offshore oil and gas industry (Wang et al., 2006; Randolph et al., 2011). In deep water environment they are employed to support subsea infrastructure, such as pipeline end manifolds and terminations, valve protection systems; and in shallow water environment to support gravity based structures. In the offshore renewable energy industry, circular buckets are recently identified as a promising foundation concept for supporting wind turbines either directly by means of a monopod, tripod or tetrapod system, or through a jacket structure. The application versatility is being broadened due to their ease of installation and cost effectiveness (Lian, 2014).

Skirted foundations are installed by pumping water from inside the skirt after they are allowed to penetrate under their self-weight. The difference between the hydrostatic water pressure outside the skirt and the reduced water pressure inside provides a differential pressure, or suction, that acts as a penetration force. This leads a deformable soil plug to be trapped inside the skirt (Vulpe, 2015).

In the operation phase, as is the focus of this paper, skirted foundations are required to withstand combined *V*-*H*-*M* (vertical-horizontal-moment) loading imposed by dead, environmental and in-service loads. The traditional methods for calculating corresponding capacity under general loading (rely on classical bearing capacity theory along with shape, depth and inclination factors; e.g. DNV, 1992; ISO, 2003) have now been superseded by three-dimensional failure envelopes, with the corresponding advantages noted by Gourvenec and Barnett (2011) and others. Along with the classical bearing capacity theory, the failure envelope method is widely used in current design for bucket foundation. However, the failure envelopes with approximating expressions

have been proposed either for clay (e.g. Ukritchon et al., 1998; Bransby and Randolph, 1999; Taiebat and Carter, 2000; Randolph and Puzrin, 2003; Gourvenec, 2008; Yun and Bransby, 2007a; Gourvenec, 2008; Bransby and Yun, 2009; Gourvenec and Barnett, 2011; Gourvenec and Mana, 2011; Martin, 2001; Barari and Ibsen, 2012; Bienen et al., 2012; Hung and Kim, 2012, 2014; Kourkoulis et al., 2014; Vulpe et al., 2013, 2014; Vulpe, 2015) or for sand (e.g. Byrne and Houlsby, 2004; Andersen et al., 2008; Ibsen et al., 2014; Park et al., 2016). As of concern, no investigation was carried out for skirted foundations on layered soils particularly on sand-over-clay, which is commonly encountered in some petroleum and renewable energy active regions e.g. in the Yellow Sea of Korea, North Sea, Gulf of Mexico, South China Sea, offshore India and Thailand. Except, Park and Park (2017), who investigated only vertical bearing capacity of skirted foundations in sand-over-clay, and the skirt was rested within the sand layer did not penetrate into the bottom clay layer.

This paper reports the results from an extensive investigation carried out to explore the kinematic failure mechanisms and capacity of skirted foundations subjected to general *V-H-M* loading with 3 degree-of-freedom (3-DOF) on sand-over-clay deposits, with the skirt tip being into the bottom clay layer. Three-dimensional (3D) small strain analyses were undertaken, varying the thickness of the sand layer relative to the foundation diameter and the skirt length relative to the sand layer thickness. Of particular interest was the effect of the surface sand layer on the capacity. Failure envelopes and approximating expressions were proposed to predict the ultimate limit states of skirted foundations in sand-over-clay under combined in-plane *V-H-M* loading.

2 NUMERICAL MODEL

2.1 *Geometry and Parameters*

Bransby and Yun (2009), Vulpe (2015) and others have showed that the soil plug trapped inside the skirt compartment during installation of the foundation significantly influence the uniaxial capacity and shape and size of the failure envelopes, leading to the necessity of simulation of a skirted foundation rather than a solid cylinder. This study has considered a circular skirted foundation of diameter D, skirt length d and skirt thickness t, founded on a sand-over-normally consolidated clay deposit, as illustrated schematically in Figure 1. The top sand layer has cohesion c, friction angle ϕ and dilation angle ψ, effective unit weight γ'_s, and thickness T_s, and the underlying clay layer has non-uniform undrained shear strength $s_u = s_{umc} + kz$, and effective unit weight γ'_c. s_{umc} is the undrained shear strength at the sand-clay interface line, k is the rate of increase of s_u with depth z (from the mudline).

In this study, the skirt length was selected as the ratio to the foundation diameter of d/D = 0.25, 0.50, 0.75 and 1.00, with relative thickness of the skirt being t/D = 0.005. The thickness of the sand layer was varied relative to the foundation diameter as T_s/D = 0.0, 0.2, 0.4 and 0.6. In all the cases, the skirt tip was placed in the clay layer. The submerged unit weight for the clay and sand layers were chosen typically with a ratio of γ'_c/γ'_s = 6/8 = 0.75. The typical effective unit weight of clay γ'_c = 6 kN/m^3 (Zhou et al., 2013; Zhou et al., 2016) and that of sand γ'_s = 8 kN/m^3 were chosen. The notation for loads and displacements are assembled in Table 1.

2.2 *Analysis Details*

All 3D small strain FE analyses were performed using the commercial FE package Abaqus/Explicit (Dassault Systèmes, 2013) because Abaqus/Explicit is more stable than Abaqus/implicit for analysis considering a sand layer with similar accuracy. The soil domain was chosen as 10*D* in diameter and 4*D* in depth beneath the tip of the installed foundation to ensure that the boundaries were well outside the plastic zone. Only a half sector of the 3D domain was involved accounting for the inherent symmetry associated with in-plane *V*, *H*, and *M* loading. A typical mesh is shown in Figure 2, representing a semi-cylindrical section through a diametrical plane of a circular skirted foundation. Based on a mesh convergence study, the typical soil element size around the skirt was adopted as 0.067*D*. The interfaces between the skirt and sand/clay was simulated using the penalty function in Abaqus (Dassault Systèmes, 2013). Common nodes connected the foundation with the soil at the foundation-soil interface, preventing any separation occurring under tension. Due to the suction developed within the soil plug trapped inside the skirt compartment, the assumption of fully bonded (i.e. fully rough) contact model for the plug soil-skirt inner surface both in sand and clay was reasonable to simplify the problem (following Bransby and Randolph, 1998; Taibet and Carter, 2000; Bransby and Yun, 2009; Huang & Kim, 2012, 2014). The interface between the soil-skirt outer surface was also assumed to be fully rough, and the detachment between the skirt and the soil was prevented (Yun and Bransby, 2007a, 2007b; Gourvenec, 2008; Bransby and Yun, 2009; Barari and Ibsen, 2012; Huang & Kim, 2012, 2014), to make the calculation more stable. Except, for the validation exercise, the interface was assumed to be smooth because the surface of the model steel caisson was anodised (and not sand blasted). Displacement boundary conditions prevented out of plane displacements of the vertical faces (i.e. the flat diametrical plane

on the front of the mesh, and around the circumference), and the base of the mesh was fixed in all three coordinate directions.

2.3 *Constitutive Law and Material Properties*

For the sand layer, the properties of the commercially available superfine silica sand that has been used in a number of investigations at the University of Western Australia were used as an abundance of reliable data regarding the geotechnical properties is readily available (Cheong, 2002; Lee et al., 2013; Teh et al., 2010; Hu et al., 2014). The poperies of the sand material are: specific gravity, G_s = 2.65; average effective particle size d_{50} = 0.19 mm; maximum void ratio, e_{max} = 0.75; minimum void ratio, e_{min} = 0.45. An elastic modulus E = 50000 kPa with cohesion c = 0.1 kPa (for maintaining numerical stability), a friction angle ϕ = 32 °, and a dilation angle ψ = 2 ° were considered for medium dense fine silica sand commonly encountered in the surface layer of seabed sediments. A Poisson's ratio of ν = 0.3 was adopted assuming drained conditions. The sand was modelled as an elastic-perfectly plastic material obeying Mohr-Coulomb yield criterion, with non-associated flow.

The clay layer was modelled as an elasto-plastic material obeying a Tresca yield criterion, with associated flow. All the analyses simulated undrained conditions and adopted a Poisson's ratio ν = 0.49 (sufficiently high to give minimal volumetric strains, while maintaining numerical stability), friction and dilation angles ϕ = ψ = 0, and a uniform stiffness ratio E/s_u =500 (where E is the Young's modulus) throughout the clay profile. The stiffness ratio is within the range commonly adopted for soft clays, but the precise value has negligible effect on the results presented. A number of values of clay strength non-homogeneity were prescribed as $\kappa_c = kD/s_{umc}$ = 0~3.0, varying the clay strength at the interface s_{umc} as 1.3~15 kPa, which are commonly encountered in the

field (Menzies and Roper, 2008). The geostatic stress conditions were modelled using K_0 = 1-sin(ϕ) = 1-sin(32°) = 0.47 for the sand layer, and K_0 = 1-sin(ϕ) = 1-sin(0°) = 1 for the clay layer (Jacky, 1944). The influence of the values of K_0 on the skirted foundation response was not investigated. It should be noted that the elastic properties (E, ν) and K_0 values have been shown to have minimal influence on the calculated bearing capacity of the foundation (Potts et al., 2001; Lee and Salgado, 2005).

2.4 *Sign Convention and Notation*

Sign conventions for loads and displacements presented in this paper obey a right-handed axes and clockwise positive convention as proposed by Butterfield et al. (1997). The adopted notations are summarised in Table 1. The ultimate loads are those for uniaxial loading (e.g. $H = M = 0$ for V_{ult}). However, for moment loading, the maximum moment (denoted by M_{max} and corresponding m_{max}) is mobilised at a positive horizontal load $H > 0$ due to the nature of offshore operational loading.

2.5 *Loading Methods and Paths*

The reference point (RP) for applying displacements was located at the centre of the circle at the skirt tip level (see Figure 1). Uniaxial vertical (V_{ult}), horizontal (H_{ult}) and moment (M_{ult}) capacities (i.e. obtained in the absence of other load components, for example V for $H = M = 0$) were obtained with displacement-controlled probes applied to the RP until failure was reached – manifested through constant load with increasing displacement.

General combined *V-H-M* loading was achieved by applying a vertical load as a direct force, after which a series of constant-ratio displacement probes of translation (u) and rotation (θ) were applied to the RP. The applied vertical load level was defined as a

proportion of the uniaxial vertical capacity (V_{ult}). The vertical load level is described by $v = V/V_{ult}$ where v took values of 0.0, 0.5 or 0.75. In general, between 10 and 15 probe tests are required to construct a failure envelope for each combination of the vertical load level, skirt length ratio and sand layer thickness ratio. Probe tests at a fixed displacement ratio give rise to load paths that approach the failure envelope from the origin. The load paths are initially following the gradients determined by the elastic stiffness of the surrounding soil. With the internal plastic yielding of the surrounding soil, the load path gradients start to change till they reach the failure envelope. All together around 350 analyses were carried out to establish failure envelopes for various loading combinations under different layered soil profiles.

The swipe test, introduced by Tan (1990), is found to be convenient to determine a complete failure envelope in a two-dimensional loading plane from a single test, which tracks a load path close to the true failure envelope under various conditions. However, in some circumstances especially for 3D loading on skirted foundations (i.e. skirt length $d/D > 0$), previous studies (e.g. Supachawarote et al., 2005) have confirmed that a swipe path may considerably undercut the true failure envelope. For this reason, swipe tests were used only for validation analyses on a surface foundation (i.e. $d/D = 0$) subjected to combined *V-H* or *V-M* loading, while the fixed-ratio displacement probe method (Bransby and Randolph, 1997) was employed to carry out all the other analyses.

2.6 *Validation*

Validation exercises were carried out against existing theoretical solutions and results from FE analyses. For a surface flat circular footing resting on clay with strength non-homogeneity $\kappa_c = 0$ and 3, analyses were carried out under uniaxial vertical displacement using implicit and explicit algorithms of Abaqus. Both smooth and rough

256 footing base were considered. The values of dimensionless uniaxial vertical capacity,
257 $v_0 = V_{ult}/As_{u0}$ (V_{ult} represents the ultimate limit state under uniaxial vertical loading, A
258 $= \pi D^2/4$, and s_{u0} is the undrained shear strength at the skirt tip level), which can be taken
259 as vertical bearing factor, N_c, from this study show very good agreement with the
260 existing solutions, as tabulated in Table 2.

261 Similar analyses were carried out for a surface flat circular footing on silica sand
262 considering $\phi = 30°$ and base roughness $\alpha = 0$, 0.2 and 1. The results from this study
263 are $N_\gamma = 7.05$, 10.18, 14.4 for $\alpha = 0$, 0.2 and 1 respectively. These values are very close
264 to the corresponding lower bound plasticity solutions of $N_\gamma = 6.935$, 9.891, 14.13
265 (Cassidy and Houlsby, 2002) with the FE results marginally higher within 3%
266 difference.

267 For a surface flat circular footing on uniform clay ($\kappa_c = 0$), 3D analyses were also
268 carried out to construct *H-M* and *V-H* envelopes. The results of this study are compared
269 with the FE results presented by Taiebat and Carter (2000) in Figure 3. Similar shapes
270 of *H-M* and *V-H* envelopes can be seen. The slight discrepancy in terms of moment
271 capacity might be due to the analysis methods used: 3D-displacement controlled
272 analysis in this study and 3D-load controlled analysis by Taiebat and Carter (2000).

273 The good agreements between the current results with the existing results of surface
274 footings on clay and sand provide confidence in the numerical model used and the
275 accuracy of the corresponding results. Furthermore, the numerical comparisons in
276 Table 2 confirm the suitability of the explicit algorithm of Abaqus used for the
277 subsequent FE analyses of skirted foundations in sand-over-clay for better convergent
278 calculation, relative to the implicit algorithm. Moreover, during the dynamic explicit
279 calculations, the time step needed to be defined appropriately to limit the ratio of the

kinematic energy to the internal energy to be < 10% of the whole model domain, resulting in a quasi-static calculation required by this study.

3 RESULTS AND DISCUSSION

3.1 *Uniaxial Capacity*

In order to explore the effect of skirted foundation embedment depth (or skirt length) and the thickness of the sand layer on the vertical bearing capacity, the foundation skirt length ratio varied as d/D = 0.00, 0.25, 0.50, 0.75 and 1.00 with the sand layer thickness as T_s/D = 0, 0.2, 0.4 and 0.6. The clay non-homogeneity κ_c ranged from 0 to 3.

The FE results of the skirted foundations on single layer non-homogeneous clay (T_s/D = 0, κ_c = 3) are plotted in Figure 4. Figure 4a shows the typical responses of the normalised vertical load V/As_{u0} against the normalised displacement w/D for various skirt length ratio d/D. It is apparent that the ultimate load and the corresponding attainment depth (with w/D < 0.1) increases with increasing d/D. The values of the ultimate vertical bearing capacity $v_{0,Ts=0} = V_{ult}/As_{u0}$ (or N_c) for each d/D were picked and are plotted in Figure 4b. The ultimate vertical bearing capacities of skirted foundations in non-homogeneous clay have been reported by Gourvenec and Mana (2001) and Hung and Kim (2014) from FE analyses and Martin (2001) from theoretical upper bound (UB) and lower bound (LB) solutions. The results for rough-based and rough-sided skirted foundations, as is the case for this study, are included in Figure 4b for comparison. Note, (i) for all of them, the values for κ_c = 3 are not given, and hence were calculated through linear interpolation from the values for the closest upper and lower range of κ_c; (ii) for Hung and Kim (2014), s_{u0} was taken as the strength at a depth

of 0.25D beneath the skirt tip level. As such, the values were adjusted according to s_{u0} at the skirt tip level. All the results from FE analyses are consistent, and nicely bracketed by the lower and upper bound solutions. The trend of increasing v_0 with increasing d/D can be approximated as

$$v_{0,Ts=0} = 8.05 + 8.64\left(\frac{d}{D}\right)\left[1 - 0.47\left(\frac{d}{D}\right)\right] \qquad \text{for } \kappa_c = 3,\ d/D \le 1.0 \qquad (1)$$

Further analyses were carried out for κ_c = 0.12~0.6, and the results are shown in Figure 4c along with existing FE results and UB and LB solutions. The values for the small range of κ_c = 0.12~0.6 fall in a tight band, and all the FE results agree reasonably and bounded by UB and LB solutions. The FE results can be best fitted as

$$v_{0,Ts=0} = 6.27 + 10.59\left(\frac{d}{D}\right)\left[1 - 0.43\left(\frac{d}{D}\right)\right] \qquad \text{for } \kappa_c = 0.12\text{~}0.6,\ d/D \le 1.0 \qquad (2)$$

The skirted foundations with skirt depth $d/D > T_s/D$ were analysed under uniaxial vertical loading. The various skirt length ratios of d/D = 0.25, 0.50, 0.75 and 1.00 were combined with sand layer thickness ratios of T_s/D = 0.1, 0.2, 0.4 and 0.6 (κ_c = 3). Figure 5a displays load-displacement responses with all cases reaching the ultimate loading at the displacement of $w/D < 0.1$. The normalised vertical capacities ($v_0 = V_{ult}/As_{u0}$) are displayed in Figure 5b as a function of T_s/D and d/D, reflecting the trend of increasing capacity with increasing skirt length and sand layer thickness. In this sand-over-non-homogeneous clay deposit, v_0 increases with increasing T_s/D partly due to the increasing contribution from the sand layer and partly owing to increasing undrained strength at the sand-clay interface and below. It can also be seen from Figure 5b that, where the sand layer is thin (i.e. $T_s/D < 0.2$), the influence of the sand layer is negligible. The values of v_0 for various T_s/D and κ_c normalised by corresponding $v_{0,Ts=0}$ (i.e. those for

$T_s/D = 0$) plotted against $x = \frac{(T_s/D)}{(d/D)^a}$ (where a is a constant) show a unique trend, which can be approximated as (Figure 5c)

$$v_0 = v_{0,Ts=0}\left[1 - 0.2x(1 - 6.55x)\right] \geq 1 \quad (3)$$

where a = 0.17 for uniaxial vertical loading with $d/D > T_s/D$. Park and Park (2017) presented a framework for assessing vertical capacities for skirted foundations in sand over clay deposits. The calculated normalised capacities using that framework, the soil properties used in this study, and skirt length equals to sand layer thickness (i.e. $d/D = T_s/D$) also converge with the trend from this study.

The FE results of the skirted foundations under uniaxial horizontal displacement are shown in Figure 6. Without the sand layer on top (i.e. T_s/D = 0.0), the ultimate horizontal capacities $h_{0,Ts=0} = H_{ult}/As_{u0}$ for various skirt length ratios of d/D = 0.25, 0.50, 0.75 and 1.00, but with κ_c = 3 and 0.12~0.6 are plotted in Figures 6a and 6b. The FE results reported by Hung and Kim (2014) for all d/D and κ_c = 3 and 0.6; and FE and UB solutions by Gourvenec (2007) and Randolph and Puzrin (2003), respectively, for d/D = 0 and regardless of κ_c show an excellent consistency. The trend of the results has an identical shape to the one in Figure 4b for uniaxial vertical loading. Thus this trend can be expressed as

$$h_{0,Ts=0} = 1 + 6.89\left(\frac{d}{D}\right)\left[1 - 0.42\left(\frac{d}{D}\right)\right] \qquad \text{for } \kappa_c = 3,\ d/D \leq 1.0 \quad (4)$$

$$h_{0,Ts=0} = 1 + 8.16\left(\frac{d}{D}\right)\left[1 - 0.39\left(\frac{d}{D}\right)\right] \qquad \text{for } \kappa_c = 0.12\sim0.6,\ d/D \leq 1.0 \quad (5)$$

All the results of h_0 for various sand layer thickness ratios, skirt lengths and clay strength non-homogeneities are depicted in Figure 6c, and can be expressed as

346 $$h_0 = h_{0,Ts=0}\left[1-0.31x\left(1-4.42x\right)\right] \geq 1 \quad (6)$$

347 where $x = \frac{(T_s/D)}{(d/D)^a}$ and a = 0.65.

348 Similarly, for a skirted foundation subjected to rotation only, the ultimate moment
349 capacities $m_{0,Ts=0} = M_{ult}/AD s_{u0}$ for T_s/D = 0.0 and for various skirt length ratios of d/D
350 = 0.25, 0.50, 0.75 and 1.00, but with κ_c = 3 and 0.12~0.6 are plotted in Figures 7a and
351 7b, respectively. The UB solutions reported by Gourvenec (2007) and Randolph and
352 Puzrin (2003) for d/D = 0 and κ_c = 3 and 0.12~0.6 (calculated through interpolation as
353 the values were given for κ_c = 0, 2 and 6) show a reasonable agreement. By comparing
354 with Figures 4b, 6a and 6b where the corresponding capacity increases convexly, values
355 of $m_{0,Ts=0}$ in Figures 7a and 7b increases concavely, which may be presented as

356 $$m_{0,Ts=0} = 0.97 + 0.35\left(\frac{d}{D}\right)\left[1+3.57\left(\frac{d}{D}\right)\right] \quad \text{for } \kappa_c = 3,\ d/D \leq 1.0 \quad (7)$$

357 $$m_{0,Ts=0} = 0.7 + \left(\frac{d}{D}\right)\left[1+1.5\left(\frac{d}{D}\right)\right] \quad \text{for } \kappa_c = 0.12\sim0.6,\ d/D \leq 1.0 \quad (8)$$

358 The trend of $m_0/m_{0,Ts=0}$ in Figure 7c is, however, similar to that in Figures 5c and 6c.
359 The best fit through the results in Figure 7c gives the following expression

360 $$m_0 = m_{0,Ts=0}\left[1+0.09x\left(1+11.56x\right)\right] \quad (9)$$

361 with $x = \frac{(T_s/D)}{(d/D)^a}$ and a = 0.52.

362 From Figures 5c~7c, clay strength non-homogeneity κ_c has negligible effect on non-
363 dimensional capacities, which is consistent to Hung and Kim (2014). As such, in the
364 following investigation, only κ_c = 3 has been considered.

365

3.2 *V-H-M Capacity*

In order to show the effect of the surface sand layer, the failure envelopes in *V-H* space (M = 0) and *V-M* space (H = 0) of skirted foundations in sand over clay with various skirt length ratios of d/D = 0.25, 0.5, 0.75, 1 and sand layer thickness ratios of T_s/D = 0.2, 0.4, 0.6 are shown in Figure 8 and Figure 9 respectively. The data points with "star" markers indicate the foundation capacity on clay (i.e. T_s/D = 0, from Figure 5, 6 or 7). Figures 8 and 9 illustrate the envelopes under ultimate states in terms of normalised loads. Similar to uniaxial capacities, for each d/D, a thin sand layer (T_s/D = 0 ~ 0.2) has little effect on the ultimate loads. This means the envelopes in both *V-H* and *V-M* spaces only expand a little (see the difference between the star markers and the curve for T_s/D = 0.2 in Figures 8 and 9). However, for a thicker sand layer with T_s/D > 0.2, the envelopes expand sharply. The interaction of the vertical and moment degrees-of-freedom (Figure 9) is slightly stronger than that in the *V-H* space (Figure 8) i.e., compared to the horizontal capacity, the moment capacity reduces more quickly with increasing vertical load.

Figure 10 shows the failure envelopes in *H-M* space (V = 0) and their dependence on sand layer thickness ratio (T_s/D) and foundation skirt length ratio (d/D). With the combination of vertical and moment loading of the foundation, the failure envelopes become oblique. The obliqueness become more server with larger skirt length. For a constant skirt length ratio, the ultimate moment loading increases with increasing sand layer thickness ratio. This is attributed to the increased capacity from the thicker sand layer and the stronger clay embedded deeper underneath the sand. As such, it is apparent that the failure envelopes are a function of both d/D and T_s/D. The envelopes for d/D = 0.5 and T_s/D = 0 from Hung and Kim (2014) have been included in Figures 8c, 9c and 10c, evidencing reasonable consistency.

3.3 *Approximating Expression*

Figure 11 represents the ultimate states normalised by the corresponding uniaxial load, $v = V/V_{ult}$, $h = H/H_{ult}$, and $m = M/M_{ult}$, indicating the shape of the relative size of the failure envelopes. First, expressions were developed for *V*-*H* and *V*-*M* envelopes. All the results presented in Figures 8 and 9 are normalised and plotted in Figures 11a and 11b respectively. The values show a unique trend in each space, regardless of skirt length ratio and the sand layer thickness ratio, which can be described using a power law respectively as.

$$h = \left(1 - v^3\right)^{1/2} \tag{10}$$

$$m = \left(1 - v^3\right)^{1/2.4} \tag{11}$$

The exponents (1/2 for Equation 10 and 1/2.4 for Equation 11) show the coupling effects between different loadings: the vertical loading has more effect on the horizontal capacity (exponent of 1/2) than on the moment loading capacity (exponent of 1/2.4). The results are in excellent agreement with the unique curves, regardless of d/D and κ_c, reported by Hung and Kim (2014).

Failure envelopes in clay were proposed for skirted foundations by Gourvnec and Barnett (2011) and hybrid foundations by Bienen et al. (2012) using FE analysis results. Randolph and House (2002) reported a failure envelope in *V*-*H* space for a suction caisson (with skirt length ratio of d/D~1.41 and the padeye at the top). These envelopes are also included in Figure 11. It can be seen that the exponents for horizontal or moment loadings are lower for skirted foundations, whereas the exponents for both vertical and horizontal or moment loadings are significantly lower for hybrid foundations.

414 Figure 12 shows the envelopes in *h*-*m** (where *m** has been calculated normalising *M*
415 by the corresponding moment *M** at *h* = 0) space with *v* = 0, indicating strong
416 dependence on *d*/*D* and T_s/D. Analyses have also been performed considering *v* = 0.5
417 and 0.75 with the aim of exploring corresponding effect on the failure envelopes and
418 combined capacity. The results are plotted in Figures 13, 14, 15, 16 for *d*/*D* = 0.25, 0.5,
419 0.75, 1.0 respectively. It is seen that for a shallow skirt length ratio of *d*/*D* = 0.25 with
420 a thin sand layer (i.e. $T_s/D \leq 0.2$), the effect of vertical mobilisation is not obvious. For
421 longer skirt length ratio $d/D \geq 0.5$, the effect of vertical loading is more prominent for
422 all values of *v*. It can be seen that a larger *h*-*m** failure envelope can be obtained for
423 higher vertical mobilisation. The similar findings have been reported for spudcan
424 foundations (Zhang et al., 2011, 2014). The data for various combinations of *d*/*D* and
425 T_s/D (as tabulated in Table 3), normalised by the corresponding value for *v* = 0 ($h_{v=0}$
426 or $m^*_{v=0}$), are plotted in Figure 17 showing a reasonably unique trend of decreasing
427 $h/h_{v=0}$ or $m^*/m^*_{v=0}$ with increasing *v*, which can be approximated as

428 $$\left(\frac{h}{h_{v=0}}\right)^{0.21} = 1 + 0.1v(1 - 2.7v) \tag{12}$$

429 $$\left(\frac{m^*}{m^*_{v=0}}\right)^{0.21} = 1 + 0.07v(1 - 3.29v) \tag{13}$$

430 For coupled *V*-*H*-*M* capacity, following Bienen et al. (2012) a conservative expression
431 can be developed combining Equations 10 and 11 as

432 $$|h|^2 + m^{*2.4} + v^3 = 1 \tag{14}$$

433 The approximation can alternatively be defined following Gourvenec and Barnett
434 (2011) and Vulpe (2015) according to

$$|h|^{\alpha} + m^{*\alpha} + 2\beta h m^{*} = 1 \quad (15)$$

where α and β are fitting parameters dependent on the foundation skirt length ratio and the sand layer thickness ratio. The values are tabulated in Table 3.

4 SUMMARY DESIGN PROCEDURE

A suggested procedure for estimating uniaxial or combined capacity for skirted foundations in sand-over-clay with the skirt tip installed in the underlying clay layer is outlined here. The procedure is based on the considered sand friction angle ϕ = 32 °, and a dilation angle ψ = 2 °, and clay undrained shear strength non-homogeneity $\kappa_c = kD/s_{umc}$ = 0.12~3.0. The procedure can be modified for other sand and clay strength properties, quantifying the corresponding effects and maintaining equivalent principles.

1. From the installation record, determine the skirt embedment depth d, and from the site specific soil investigation report, determine the sand layer thickness T_s.
2. For the given foundation diameter D, calculate d/D and T_s/D.
3. Calculate uniaxial vertical load capacity v, horizontal load capacity h and moment capacity m using Equations 3, 6 and 9 respectively.
4. Establish v-h and m-h failure envelopes using Equations 10 and 11, respectively, with the effect of vertical mobilisation quantified using Equations 12 and 13, respectively.
5. Estimate v-h-m^* capacity using Equations 14 or 15 with the corresponding constants in Table 3.

5 CONCLUDING REMARKS

A series of small strain FE analyses were carried out on circular skirted foundations installed in the underlying clay layer of sand-over-non-homogeneous clay deposits. The combined capacity of a foundation was shown to be a function of the sand layer thickness ratio, foundation skirt length ratio and vertical load mobilisation level. The following key conclusions can be drawn from the results presented in this paper.

a) Uniaxial vertical, horizontal and moment load capacities of skirted foundations on sand-over-clay deposits, normalised by the corresponding capacity in the absence of the sand layer, showed unique trend against $\frac{(T_s / D)}{(d / D)}$. Equations 3, 6 and 9 can be used to calculate the capacities respectively.

b) Failure envelope in either *V-H* or *V-M* space expanded very slowly up to the sand layer thickness of $T_s/D = 0.2$, and then sharply for $T_s/D > 0.2$. The interaction of the vertical and moment degrees-of-freedom was slightly stronger than that in the *V-H* space i.e., compared to the horizontal capacity, the moment capacity reduces more quickly with increasing vertical load.

c) For any vertical load mobilisation level (*v*), all results converge on *v-h* and *v-m* spaces regardless of the sand layer thickness ratio and skirt length ratio. The normalised failure envelopes were expressed by Equations 10 and 11 respectively.

d) Complex interaction on *h-m** space resulted non-unique normalised failure envelopes with strong dependence on the sand layer thickness ratio, skirt length ratio, and vertical load mobilisation level. Nonetheless, expressions (Equations 14 and 15) were proposed to approximate the failure envelopes.

The proposed expressions will enable practitioners to derive the failure envelopes in the field during preliminary design. The design framework was established based on the properties of a silica sand with friction angle = 32 °and dilation angle = 2 °with no particle breakage. Caution should be exercised for applying the framework for sands with other friction and dilation angles and for other sands with potential particle breakage.

6 ACKNOWLEDGEMENTS

The research presented here was undertaken with support from the Australian Research Council (ARC) Discovery Grant (DP1096764), the National Natural Science Foundation of China (Grant No. 51378197 & No. 51578231) and supported by the Fundamental Research Funds for the Central Universities of China (D2171820),Water conservancy science and technology innovation project of Guangdong province(2015-17), Science and Technology Program of POWERCHINA Huadong Engineering Corporation Limited （SD2013-10） and Science and Technology Program of Guangzhou (201707020047).The work forms part of the activities of the Centre for Offshore Foundation Systems (COFS), currently supported as a node of the Australian Research Council Centre of Excellence for Geotechnical Science and Engineering and as a Centre of Excellence by the Lloyd's Register Foundation. This support is gratefully acknowledged, as is the benefit of discussion with Dr Long Yu, Dr Dong Wang and Dr Xu Li.

501

502

503

7 REFERENCES

Andersen, K. H., Jostad, H. P. Dyvik, R. 2008. Penetration resistance of offshore skirted foundations and anchors in dense sand. J. Geotech. Geoenvironmental Eng. ASCE, 134(1), 106-116.

Barari, A. Ibsen, L. B. 2012. Undrained response of bucket foundations to moment loading. Applied Ocean Research, 36, 12-21.

Barari, A. Ibsen, L. B. 2012. Undrained response of bucket foundations to moment loading. Applied Ocean Research, 36(3), 12-21.

Bienen, B., Gaudin, C., Cassidy, M.J., Rausch, L., Purwana, O.A. Krisdani, H. 2012. Numerical modelling of a hybrid skirted foundation under combined loading. Computers and Geotechnics, 45, 127-139.

Bransby, M. Randolph, M.F.1997. Shallow foundations subject to combined loadings. Proceedings of the 9th International Conference on Computer Methods and Advances in Geomechanics. Wuhan, November. Edited by J. Yuan. AA Balkema, Rotterdam, pp. 1947-1952.

Bransby, M. Randolph, M.F. 1998. Combined loading of skirted foundations. Géotechnique, 48(5), 637-655.

Bransby, M. Randolph, M.F. 1999. The effect of skirted foundation shape on response to combined VMH loadings. International Journal of Offshore and Polar Engineering, 9(3).

Bransby, M. Yun, G.J. 2009. The undrained capacity of skirted strip foundations under combined loading. Géotechnique, 59(2), 115-125.

Barari, A. and L. B. Ibsen. 2012. Undrained response of bucket foundations to moment

527 loading. Applied Ocean Research, 36 12-21.

528 Butterfield, R., Houlsby, G.T. Gottardi, G. 1997. Standardized sign conventions and
529 notation for generally loaded foundations. Géotechnique, 47(5), 1051-1054.

530 Byron, W. B. Houlsby, G.T. 2004. Experimental Investigations of the response of
531 suction caissons to transient combined loading. J. Geotech. Geoenvironmental
532 Eng., ASCE, 130(3), 240-253.

533 Cheong,J. 2002. Physical testing of jack-up footings on sand subjected to torsion.
534 Honours thesis, University of Western Australia, Perth, Australia.

535 Cox, A. D. Eason, G. Hopkins, H. G. 1961. Axially symmetric plastic deformations in
536 soils. Philosophical Transactions of the Royal Society A Mathematical Physical
537 & Engineering Sciences, 254(1036), 1-45.

538 Jacky, J. 1944. The coefficient of earth pressure at rest. In Hungarian (A nyugalmi
539 nyomas tenyezoje). Journal of the Society of Hungarian Architects and
540 Engineers, Budapest, Hungry, 355-358.

541 Lee, J., Salgado, R., 2005. Estimation of bearing capacity of circular footings on sands
542 based on cone penetration test. Journal of Geotechnical and Geoenvironmental
543 Engineering 131(4), 442-452.

544 Lee, K.K. Cassidy, M.J., Randolph, M.F. 2013Bearing capacity on sand overlying clay
545 soils:Experimental and finite element investigation of potential punch-through
546 filure, geotechnique 63(15)1271-1284

547 Lian, J., Chen, F., Wang, H. 2014. Laboratory tests on soil–skirt interaction and
548 penetration resistance of suction caissons during installation in sand. Ocean
549 Engineering, 84(3), 1-13.

550 DNV (Det Norske Veritas) 1992. Foundations, classifications notes no. 30.4. Oslo,
551 Norway.Gourvenec, S.M. 2007. Failure envelopes for offshore shallow
552 foundations under general loading. Géotechnique 57(9), 715-728.

553 Houlsby, G.T., Martin, C.M., 2003. Undrained bearing capacity factors for conical
554 footings on clay. Géotechnique 53(5), 513-520.

555 Hung L.C., Kim S.R., 2012. Evaluation of vertical and horizontal bearing capacities of
556 bucket foundations in clay. Ocean Engineering 52, 75-82.

557 Hung L.C., Kim S.R., 2014. Evaluation of undrained bearing capacities of bucket
558 foundations under combined loads. Marine Georesources & Geotechnology 32,
559 76-92.

560 Randolph, M. F. Puzrin A (2003)Upper bound limit analysis of circular foundations on
561 clay under general loading. Géotechnique 53.9:785-796.

562 Gourvenec, S. (2007). Failure envelopes for offshore shallow foundations under
563 general loading Geotechnique 57, No. 9, 715–728 Gourvenec, S.M. 2008.
564 Effect of embedment on the undrained capacity of shallow foundations under
565 general loading. Géotechnique 58(3), 177-185.

566 Gourvenec, S.M, Mana, D.S.K., 2011. Undrained vertical bearing capacity factors for
567 shallow foundations. Géotechnique Letters 1, 101-108.

568 Gourvenec, S.M., Randolph, M.F. 2003. Effect of strength non-homogeneity on the
569 shape of failure envelopes for combined loading of strip and circular
570 foundations on clay. Géotechnique53(6), 575-586.

571 Gourvenec, S. 2008. Effect of embedment on the undrained capacity of shallow
572 foundations under general loading. Geotechnique 58(3): 177–185.

573 Gourvenec, S. M. Barnett, S. 2011. Undrained failure envelope for skirted foundations
574 under general loading.Géotechnique61(3), 263-270.

575 Hu,P. Stanier, S.A., Cassidy,M.J., Wang D. 2014 Predicting peak resistance of spudcan
576 penetrating sand overlying clay, J. Geotech. Geoenviron. Eng.,140(2)04013009

577 Ibsen, L. B., Larsen, K. A. Barari, A. 2014. Calibration of failure criteria for bucket
578 foundations on drained sand under genral loading. J. Geotech.
579 Geoenvironmental Eng.ASCE140(7), 04014033.

580 ISO (International Standadization Organization) 2003. ISO 19901-4: Petroleum and
581 natural gas industries - specific requirements for offshore structures - Part 4:
582 Geotechnical and foundationn design considerations, 1st Ed., Geneva,
583 Switzerland.

584 Kourkoulis, R.S., Lekkakis, P.C., Gelagoti, F.M. Kaynia, A.M. 2014. Suction caisson
585 foundations for offshore wind turbines subjected to wave and earthquake
586 loading: effect of soil-foundation interface. Géotechnique64(3), 171-185.

587 Park, J.S., Park, D., Yoo, J.K. 2016. Vertical bearing capacity of bucket foundations in
588 sand. Ocean Engineering 121, 453-461.

589 Park, J.S., Park, D., 2017. Vertical bearing capacity of bucket foundation in sand
590 overlying clay. Ocean Engineering 134, 62-76.

591 Potts, D.M. Zdravkovic, L., Zdravković, L., 2001. Finite element analysis in
592 geotechnical engineering: application. Thomas Telford.

593 Randolph, M.F. House, A.R. 2002. Analysis of Suction Caisson Capacity in Clay.
594 Offshore Technology Conference.

595 Randolph, M. F., Gaudin, C., Gourvenec, S. M., White, D. J., Boylan, N., Cassidy, M.
596 J. 2011. Recent advances in offshore geotechnics for deep water oil and gas
597 developments. Ocean Engineering, 38(7), 818-834.

598 Simulia D.S., 2013. ABAQUS Documentation v6.13, Dassault Systemes Simulia
599 Corp., Providence, RI, USA.Abaqus 2013. ABAQUS Documentation, Dassault
600 Systemes, Providence, RI

601 Supachawarote, C., Randolph, M.F. Gourvenec, S.M. 2005. The effect of crack
602 formation on the inclined pull-out capacity of suction caissons. Proc. 11th Int.
603 Assoc. for Computer Methods and Advances in Geomechanics Conf., Turin, pp.
604 577-584.

605 Taiebat, H.A. Carter, J.P. 2000. Numerical studies of the bearing capacity of shallow
606 foundations on cohesive soil subjected to combined loading.
607 Géotechnique**50**(4), 409-418.

608 Tan, F.S.C. 1990. Centrifuge and theoretical modelling of conical footings on sand,
609 University of Cambridge.

610 Tani, K. Craig, W. 1995. Bearing capacity of circular foundations on soft clay of
611 strength increasing with depth. Soils and Foundations35(4), 21-35.

612 Teh K.L., Leung, C.F., Chow, Y.K., Caissdy, M.j. Quah,M. 2010 Centrifuge model
613 study of spudcan penetration in sand overlying clay. Geotechnique,60(11),825-
614 842

615 Ukritchon, B., Whittle, A.J. Sloan, S.W. 1998. Undrained limit analyses for combined
616 loading of strip footings on clay. Journal of Geotechnical and
617 Geoenvironmental Engineering124(3), 265-276.

618 Vulpe, C. 2015. Design method for the undrained capacity of skirted circular
619 foundations under combined loading: effect of deformable soil plug.
620 Geotechnique65(8), 669-83.

621 Vulpe, C., Bienen, B. Gaudin, C. 2013. Predicting the undrained capacity of skirted
622 spudcans under combined loading. Ocean Engineering74, 187-188.

623 Vulpe, C., Gourvenec, S.M. Power, M. 2014. A generalised failure envelope for
624 undrained capacity of circular shallow foundations under general loading.
625 Geotechnique Letters4(3), 187-196.

626 Wang, Y., Lu, X., Wang, S., Shi, Z. 2006. The response of bucket foundation under
627 horizontal dynamic loading. Ocean Engineering, 33(7), 964-973.

628 Yun, G.J. Bransby, M.F. 2007a. The horizontal-moment capacity of embedded
629 foundations in undrained soil. Canadian Geotechnical Journal, 44(4), 409-427.

630 Yun, G. and M. F. Bransby. 2007b. The undrained vertical bearing capacity of skirted
631 foundations. Soils and Foundations 47(3), 493–506.

632 Zhang, Y., Bienen, B., Cassidy, M. J., Gourvenec, S. 2011. The undrained bearing
633 capacity of a spudcan foundation under combined loading in soft clay. Marine
634 Structures, 24(4), 459-477.

635 Zhang, Y., Bienen, B., Cassidy, M. J. 2014. Jack-up push-over analyses featuring a new
636 force resultant model for spudcans in soft clay. Ocean Engineering, 81(2), 139-
637 149.

638 Zhou M, Hossain MS, Hu Y and Liu HL 2013. Behaviour of Ball Penetrometers in
639 Uniform and Layered Clays, Geotechnique 63(8) 682-694

640 Zhou M, Hossain MS, Hu Y and Liu HL 2016. Scale Issues and Interpretation of Ball
641 Penetration in Stratified Deposits in Centrifuge Testing, Journal of geotechnical
642 and Geoenviroment Engineering. 142(5

643 **Table 1 Notation for loads and displacements**

644

	Vertical	**Horizontal**	**Rotational**
Load	V	H	M
Ultimate load	V_{ult}	H_{ult}	M_{ult}
Dimensionless load	V/As_{u0}	H/As_{u0}	M/ADs_{u0}
Dimensionless ultimate load	$v_0=V_{ult}/As_{u0}$	$h_0=H_{ult}/As_{u0}$	$m_0=M_{ult}/ADs_{u0}$
Normalised load	$v=V/V_{ult}$	$h=H/H_{ult}$	$m=M/M_{ult}$ $m^*=M/M^*$
Displacement	w	u	θ

645

646

647

Table 2 Solutions for surface circular footings subjected to uniaxial vertical loading

Clay strength non-homogeneity, $\kappa_c = kD/s_{um}$	**Interface roughness**	**Dimensionless uniaxial vertical capacity, $v_0 = V_{ult}/As_{u0}$, which can be taken as bearing capacity factor, N_c**	
0	Smooth	Tani and Craig (1995)	5.69
		Taiebat and Carter (2000)	5.70
		Houlsby and Martin (2003)	5.69
		Gourvenec and Mana (2011)	5.549
		This study (Implicit)	**5.602**
0	Rough	Cox et al. (1961)	6.05
		Tani and Craig (1995)	6.34
		Gourvenec and Randolph (2003)	5.91
		Houlsby and Martin (2003)	6.05
		This study (Implicit)	**6.011**
		This study (Explicit)	**6.086**
3	Rough	Houlsby and Martin (2003)	8.21
		Gourvenec and Randolph (2003)	8.04
		This study (Implicit)	**8.028**
		This study (Explicit)	**8.051**

653 **Table 3 Values of α and β for Equation 15**

T_s/D	d/D	v	H_{ult} (kN)	M^* (kN.m)	α	β
0	1.00	0	5.071	2.565	1.834	-0.714
0	0.75	0	4.411	1.948	1.850	-0.675
0	0.50	0	3.633	1.462	1.715	-0.582
0	0.25	0	2.785	1.118	1.947	-0.349
0.1	0.25	0	2.742	1.19	2.032	-0.409
0.2	1.00	0	5.121	2.950	1.855	-0.741
0.2	0.75	0	4.506	2.081	1.669	-0.660
0.2	0.50	0	3.814	1.570	1.682	-0.624
0.2	0.25	0	3.210	1.310	2.139	-0.578
0.4	1.00	0	5.494	3.314	1.940	-0.824
0.4	0.75	0	5.130	2.500	1.755	-0.712
0.4	0.50	0	4.958	1.920	1.667	-0.640
0.4	0.25	0	3.210	1.310	1.977	-0.508
0.6	1.00	0	6.494	3.950	1.973	-0.869
0.6	0.75	0	6.646	3.150	1.947	-0.822
0.1	0.25	0.50	2.403	1.080	2.091	-0.417
0.1	0.25	0.75	2.119	0.900	2.046	-0.454
0.2	0.25	0.50	2.911	1.240	1.883	-0.534
0.2	0.25	0.75	2.650	1.030	1.601	-0.523
0.2	0.50	0.50	3.619	1.480	1.609	-0.604
0.2	0.50	0.75	2.909	1.180	1.709	-0.658
0.4	0.50	0.50	4.292	1.520	1.238	-0.541
0.4	0.50	0.75	3.200	1.250	1.812	-0.760
0.2	0.75	0.50	4.107	1.900	1.682	-0.670
0.2	0.75	0.75	3.301	1.600	1.622	-0.662
0.4	0.75	0.50	4.531	2.000	1.659	-0.682
0.4	0.75	0.75	3.952	1.630	1.571	-0.637
0.6	0.75	0.50	6.090	2.780	1.770	-0.737
0.6	0.75	0.75	4.870	2.350	2.078	-0.968
0.2	1.00	0.50	4.811	2.650	1.680	-0.677

0.2	1.00	0.75	3.895	2.100	1.830	-0.762
0.4	1.00	0.50	5.084	2.900	1.918	-0.838
0.4	1.00	0.75	3.968	2.400	2.181	-1.037
0.6	1.00	0.50	5.247	3.450	1.986	-0.901
0.6	1.00	0.75	3.872	2.900	1.879	-0.830

654

Number of Figures: 17

Figure 1 Schematic diagram of a skirted foundation subjected to *V-H-M* loading in sand-over-clay

Figure 2 Typical mesh used in FE analyses

Figure 3 Failure envelopes of surface circular footing on uniform clay (d/D = 0, T_s/D = 0, κ_c = 0): (a) Failure envelopes in *H-M* space (V = 0); (b) Failure envelopes in *V-H* space (M = 0)

Figure 4 Skirted foundation in clay under uniaxial vertical loading: (a) Typical vertical load-displacement response in clay (T_s/D = 0, κ_c = 3); (b) Ultimate uniaxial vertical load (T_s/D = 0, κ_c = 3); (c) Ultimate uniaxial vertical load (T_s/D = 0, κ_c = 0.12~0.6)

Figure 5 Skirted foundations in sand-over-clay under uniaxial vertical loading: (a) Vertical load-displacement response (κ_c = 3); (b) Ultimate uniaxial vertical load (κ_c = 3); (c) Normalised ultimate uniaxial vertical load (κ_c = 0.12~3)

Figure 6 Skirted foundations under uniaxial horizontal loading: (a) Ultimate uniaxial horizontal load in clay (T_s/D = 0, κ_c = 3); (b) Ultimate uniaxial horizontal load in clay (T_s/D = 0, κ_c = 0.12~0.6); (c) Normalised ultimate uniaxial horizontal load in sand-over-clay (κ_c = 0.12~3)

Figure 7 Skirted foundations under uniaxial moment loading: (a) Ultimate uniaxial moment load in clay (T_s/D = 0, κ_c = 3); (b) Ultimate uniaxial moment load in clay (T_s/D = 0, κ_c = 0.12~0.6); (c) Normalised ultimate uniaxial moment load in sand-over-clay (κ_c = 0.12~3)

678 **Figure 8** Failure envelopes in *V*-*H* space: (a) d/D = 1.0; (b) d/D = 0.75; (c) d/D =
679 0.5; (d) d/D = 0.25

680 **Figure 9** Failure envelopes in *V*-*M* space: (a) d/D = 1.0; (b) d/D = 0.75; (c) d/D =
681 0.5; (d) d/D = 0.25

682 **Figure 10** Failure envelopes in *H*-*M* space: (a) d/D = 1.0; (b) d/D = 0.75; (c) d/D =
683 0.5; (d) d/D = 0.25

684 **Figure 11** Normalised failure envelopes: (a) *v*-*h* space; (b) *v*-*m* space

685 **Figure 12** Normalised failure envelopes in *h*-*m* space (v = 0): (a) d/D = 1.0; (b) d/D
686 = 0.75; (c) d/D = 0.5; (d) d/D = 0.25

687 **Figure 13** Effect of vertical mobilisation *v* on normalised failure envelopes in *h*-*m*
688 space: d/D = 0.25: (a) T_s/D = 0.1; (b) T_s/D = 0.2

689 **Figure 14** Effect of vertical mobilisation *v* on normalised failure envelopes in *h*-*m*
690 space: d/D = 0.5: (a) T_s/D = 0.2; (b) T_s/D = 0.4

691 **Figure 15** Effect of vertical mobilisation *v* on normalised failure envelopes in *h*-*m*
692 space: d/D = 0.75: (a) T_s/D = 0.2; (b) T_s/D = 0.4; (c) T_s/D = 0.6

693 **Figure 16** Effect of vertical mobilisation *v* on normalised failure envelopes in *h*-*m*
694 space: d/D = 1.0: (a) T_s/D = 0.2; (b) T_s/D = 0.4; (c) T_s/D = 0.6

695 **Figure 17** Design charts for quantifying effect of vertical mobilisation *v*: (a) *v*-*h*
696 space; (b) *v*-*m** space

697

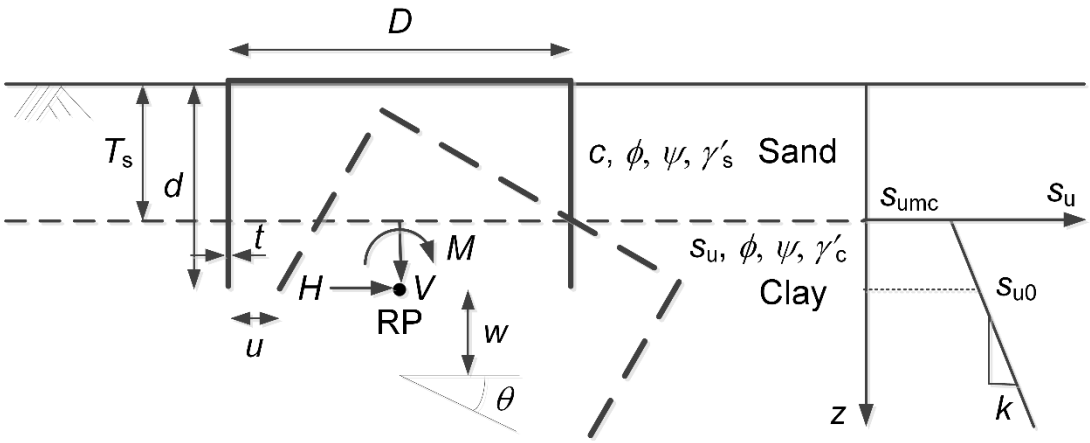

698

699

700 **Figure 1 Schematic diagram of a skirted foundation subjected to *V*-*H*-*M* loading**

701 **in sand-over-clay**

702

703

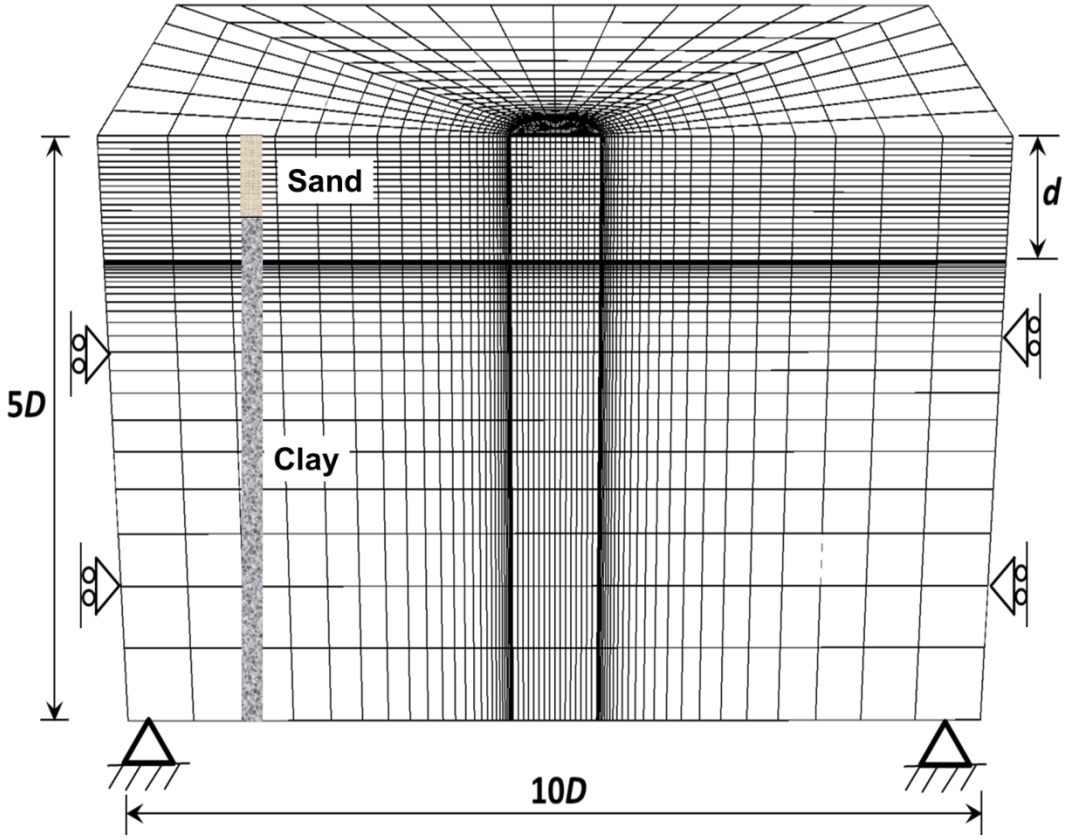

704

705 **Figure 2 Typical mesh used in FE analyses**

706
707
708

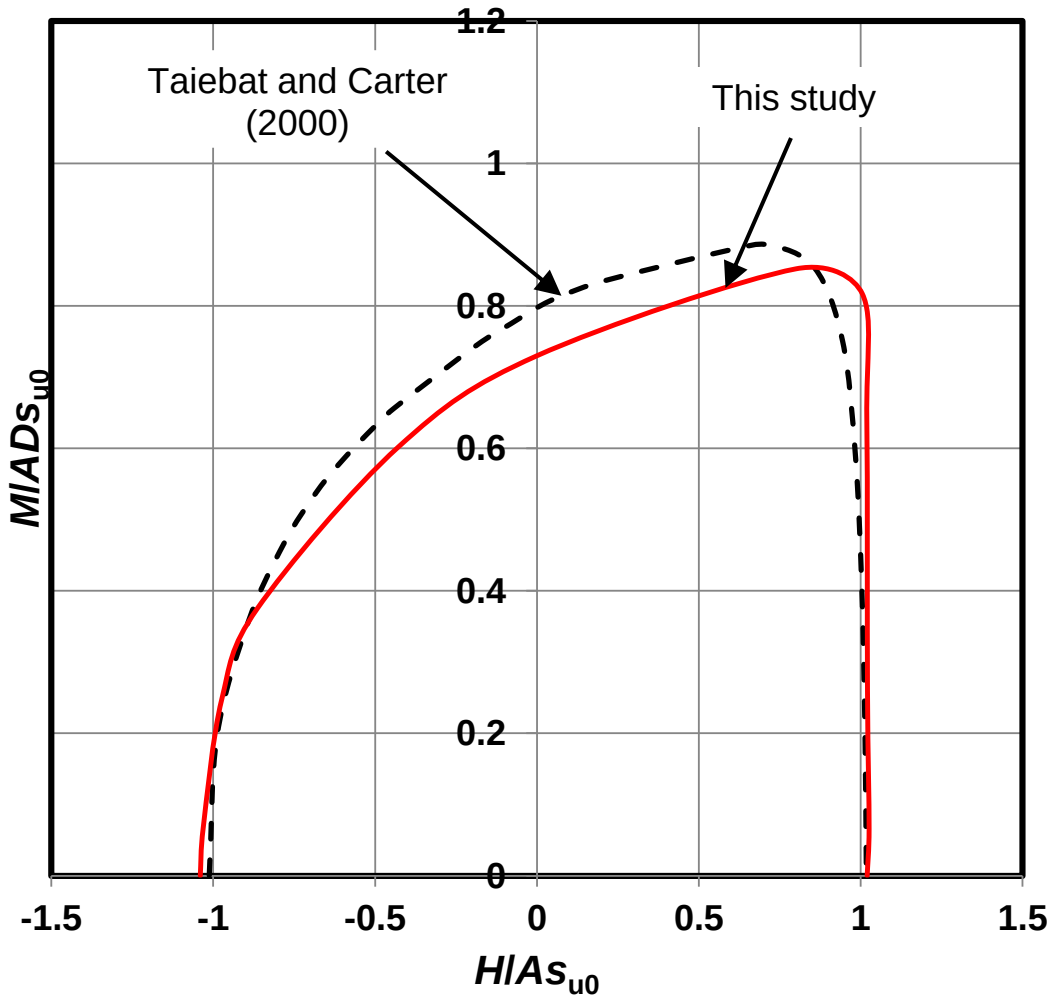

(a) Failure envelopes in H-M space ($V = 0$)

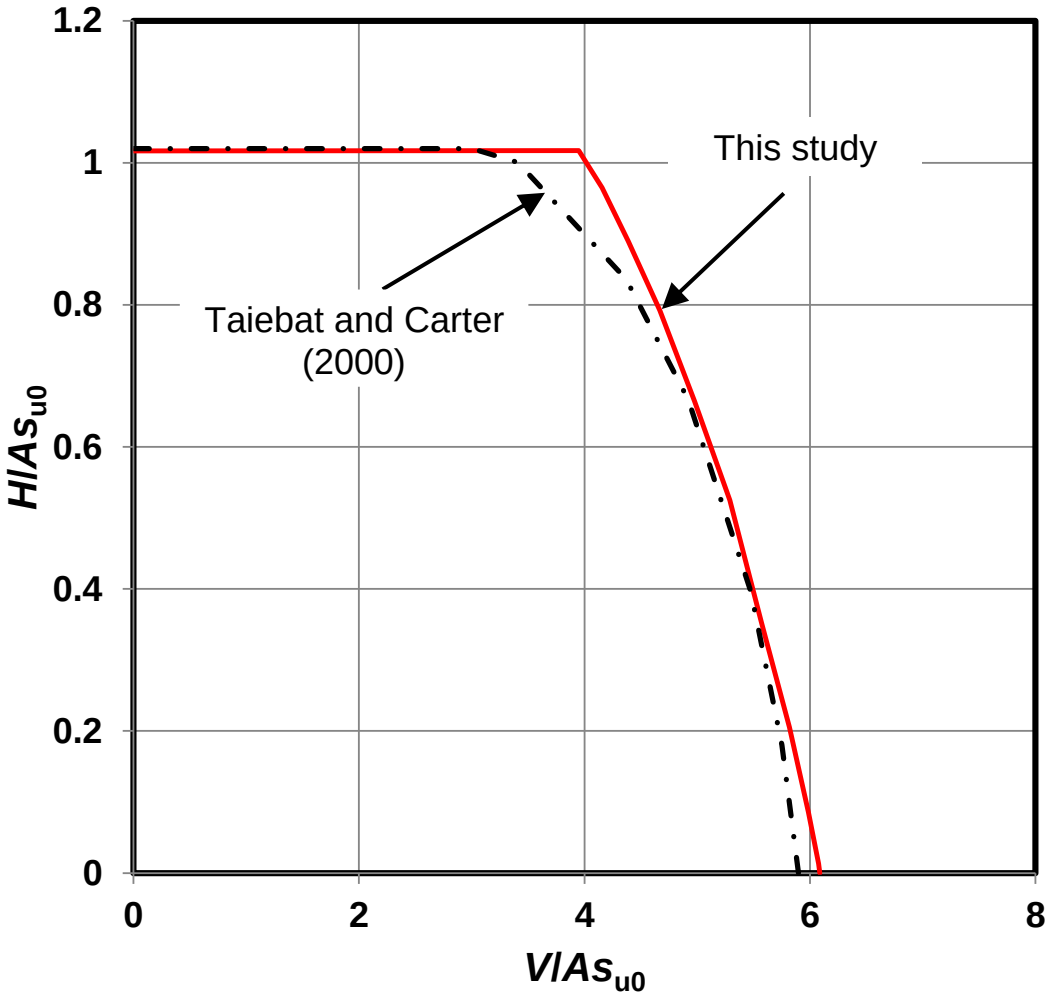

715

716 (b) Failure envelopes in *V*-*H* space (*M* = 0)

717

718 **Figure 3 Failure envelopes of surface circular footing on uniform clay (*d*/*D* = 0,**

719 **T_s/D = 0, κ_c = 0)**

720

721

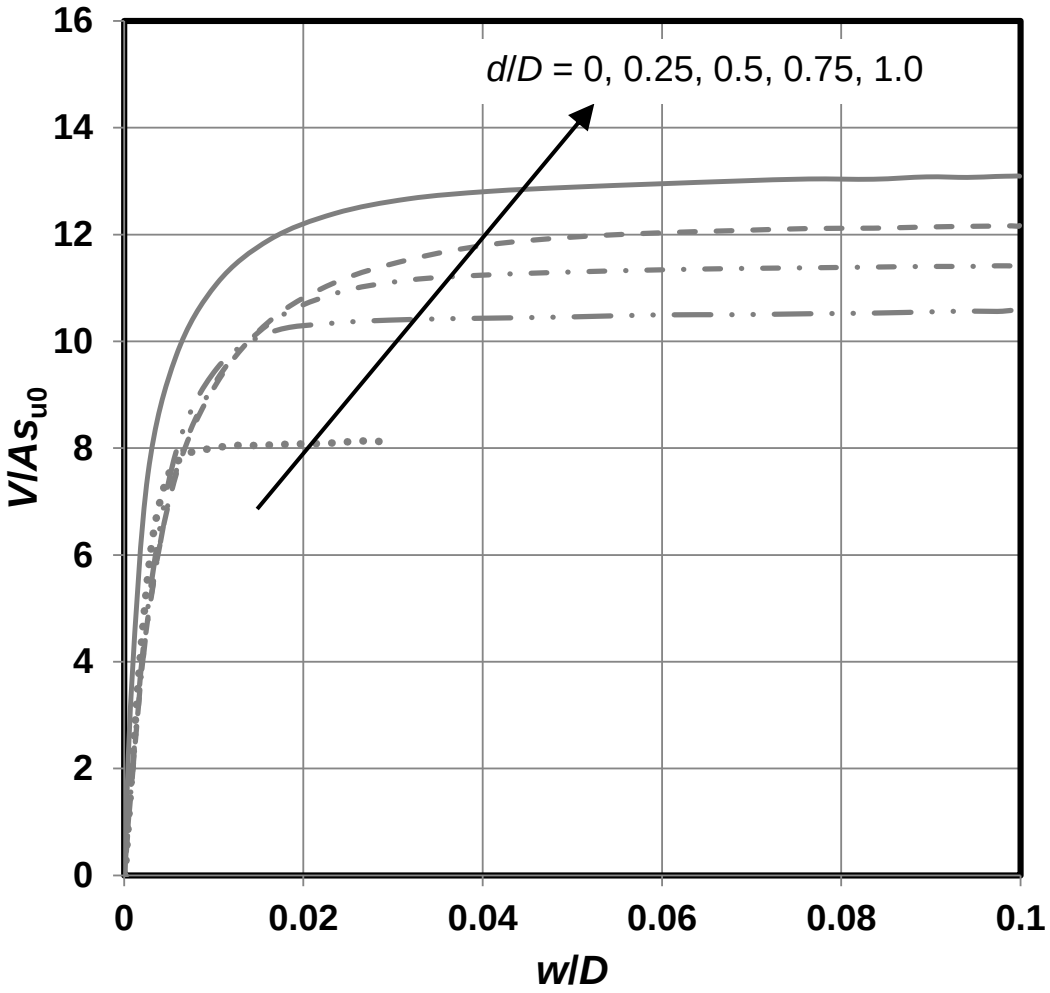

722

723 (a) Typical vertical load-displacement response in clay (T_s/D = 0, κ_c = 3)

724

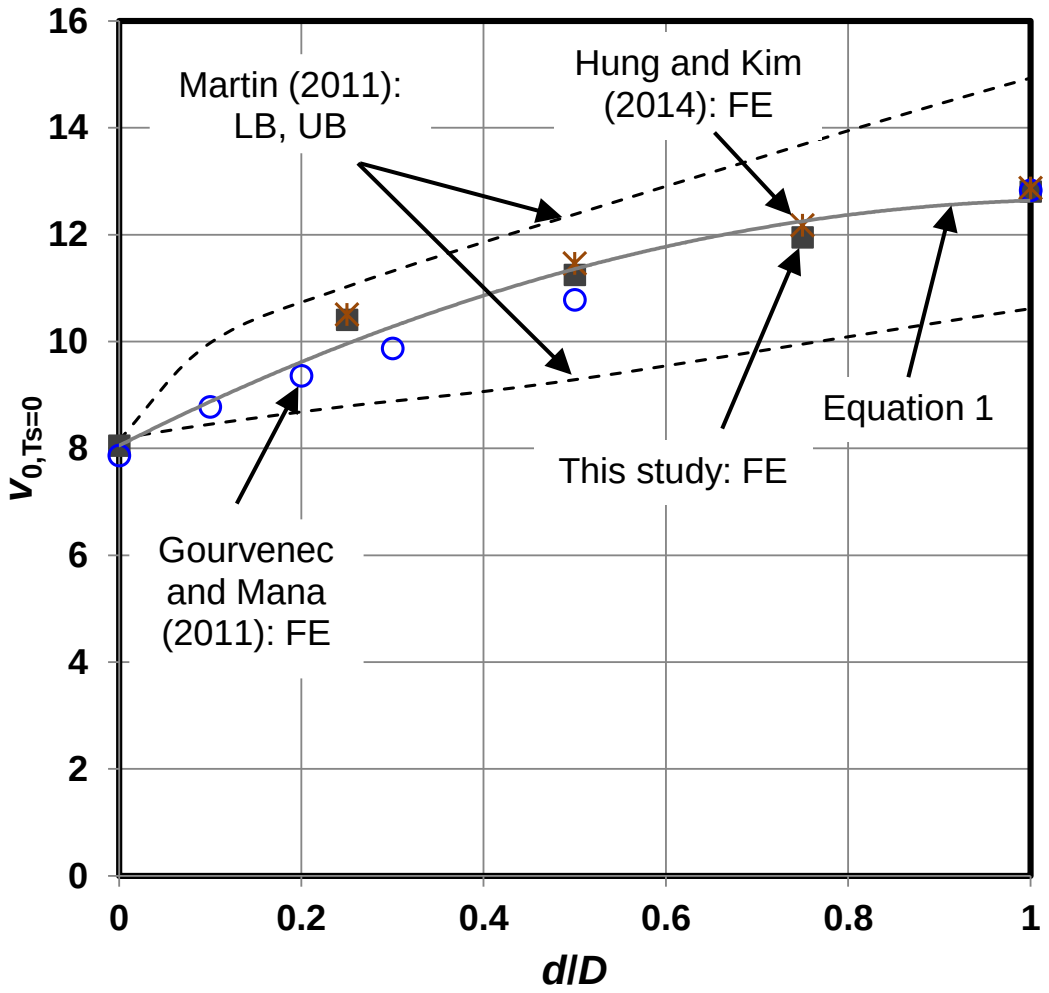

725

726 (b) Ultimate uniaxial vertical load (T_s/D = 0, κ_c = 3)

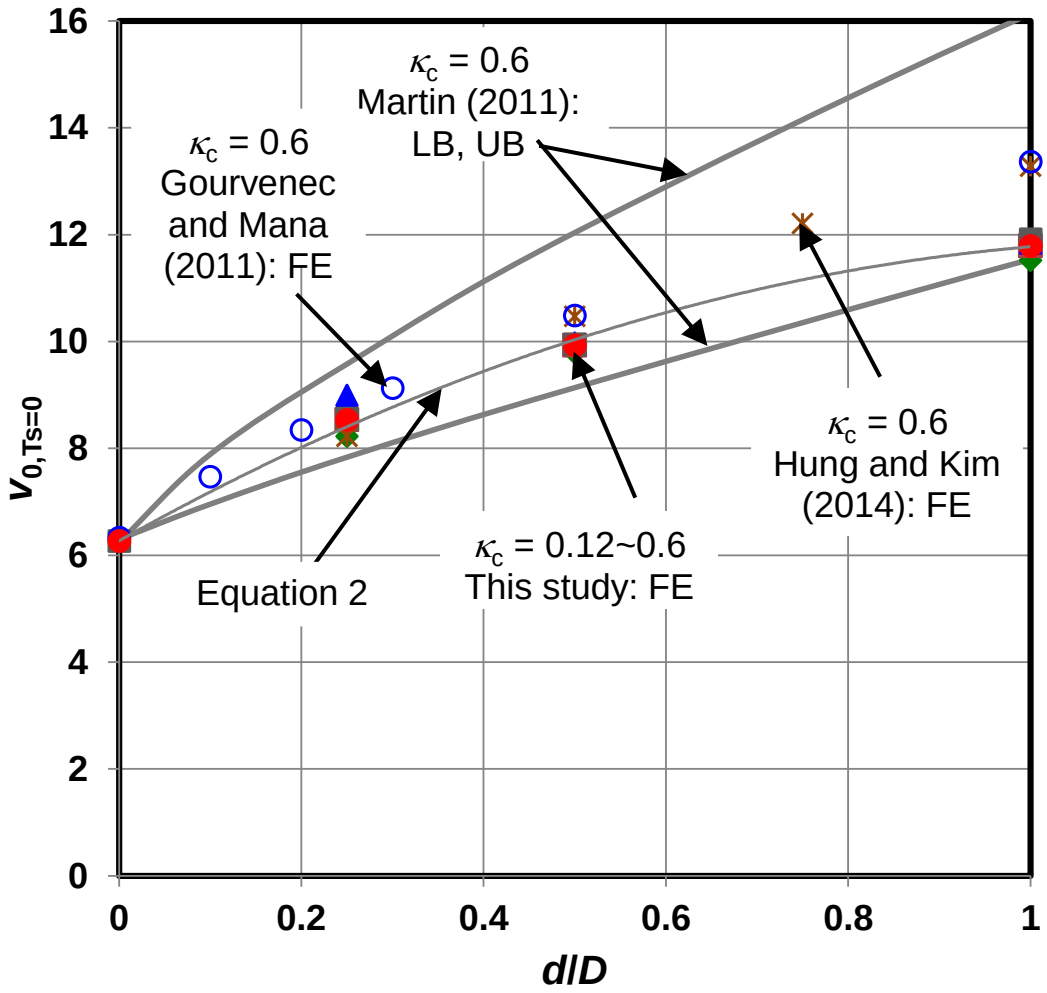

727

728 (c) Ultimate uniaxial vertical load (T_s/D = 0, κ_c = 0.12~0.6)

729 **Figure 4 Skirted foundation in clay under uniaxial vertical loading**

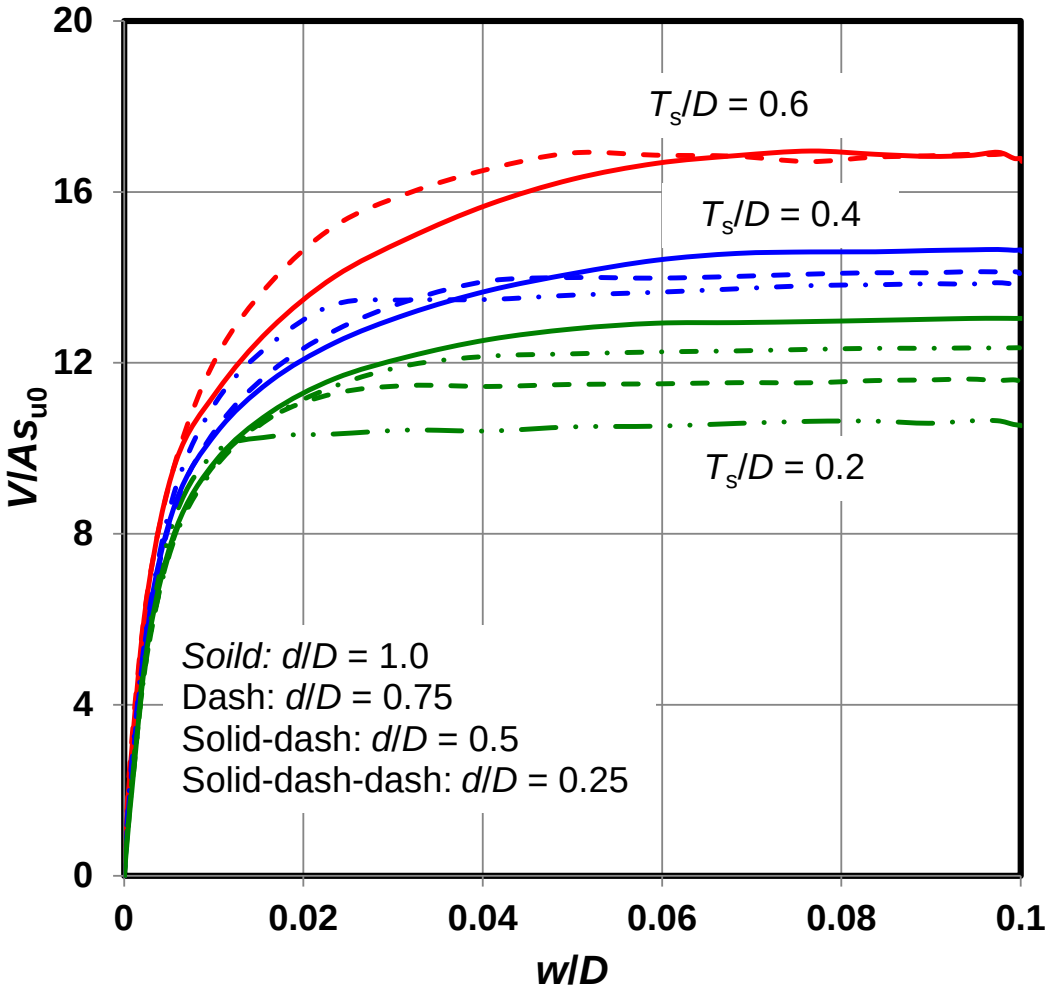

730

731 (a) Vertical load-displacement response (κ_c = 3)

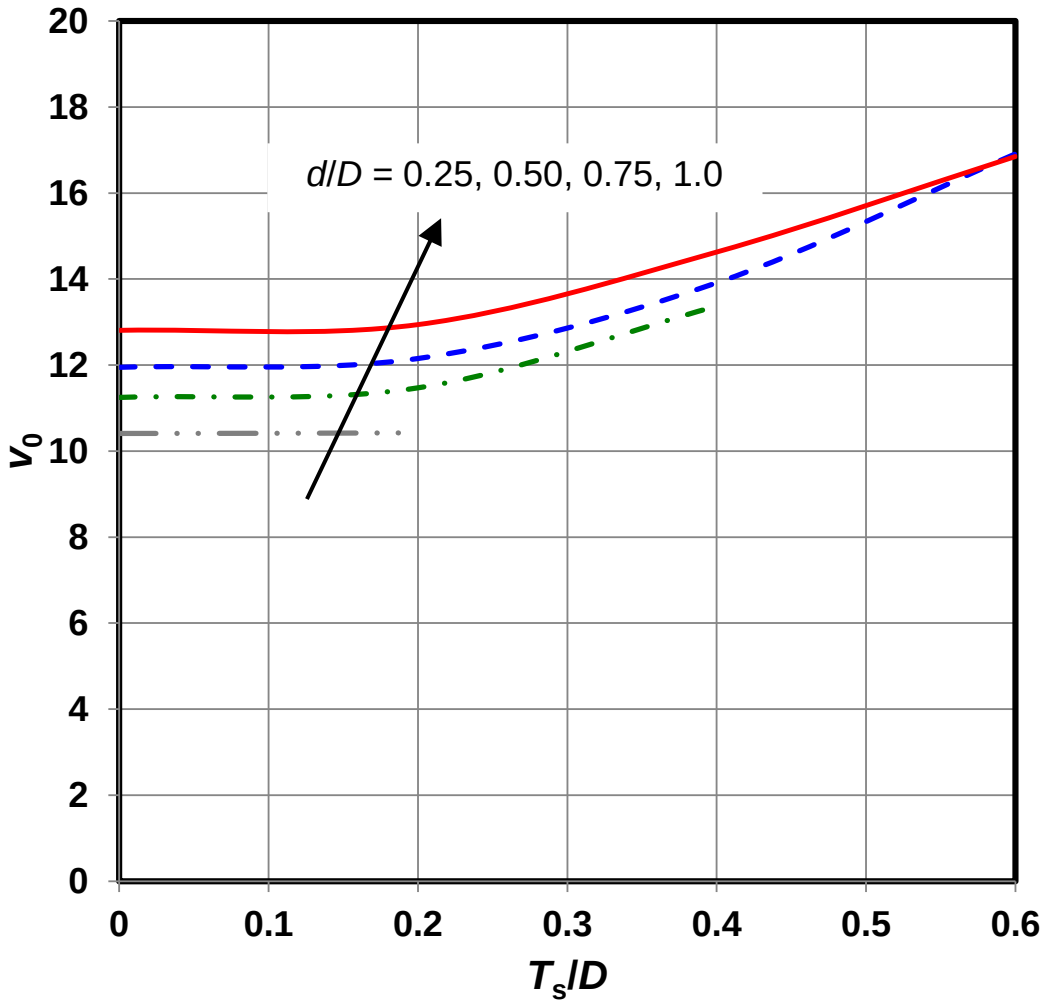

732

733 (b) Ultimate uniaxial vertical load (κ_c = 3)

734

735

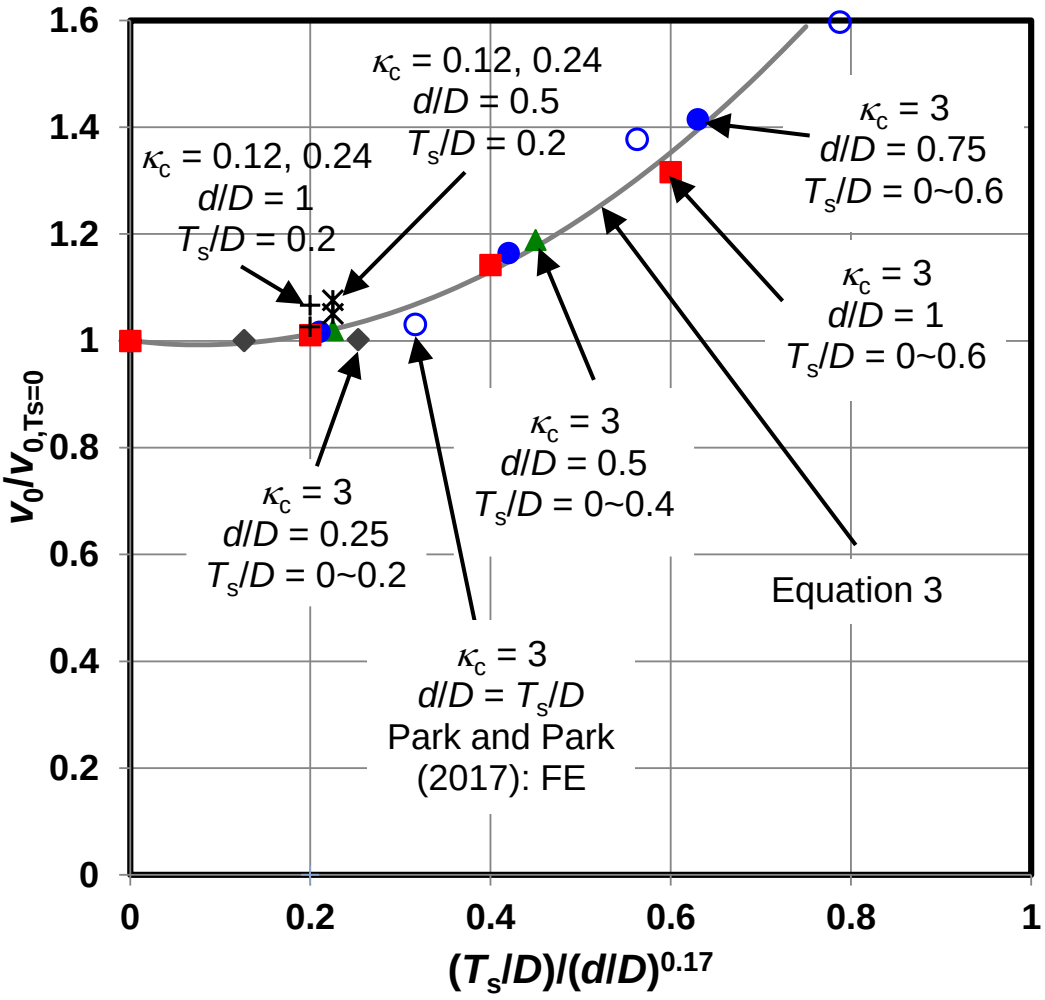

(c) Normalised ultimate uniaxial vertical load (κ_c = 0.12~3)

Figure 5 Skirted foundations in sand-over-clay under uniaxial vertical loading

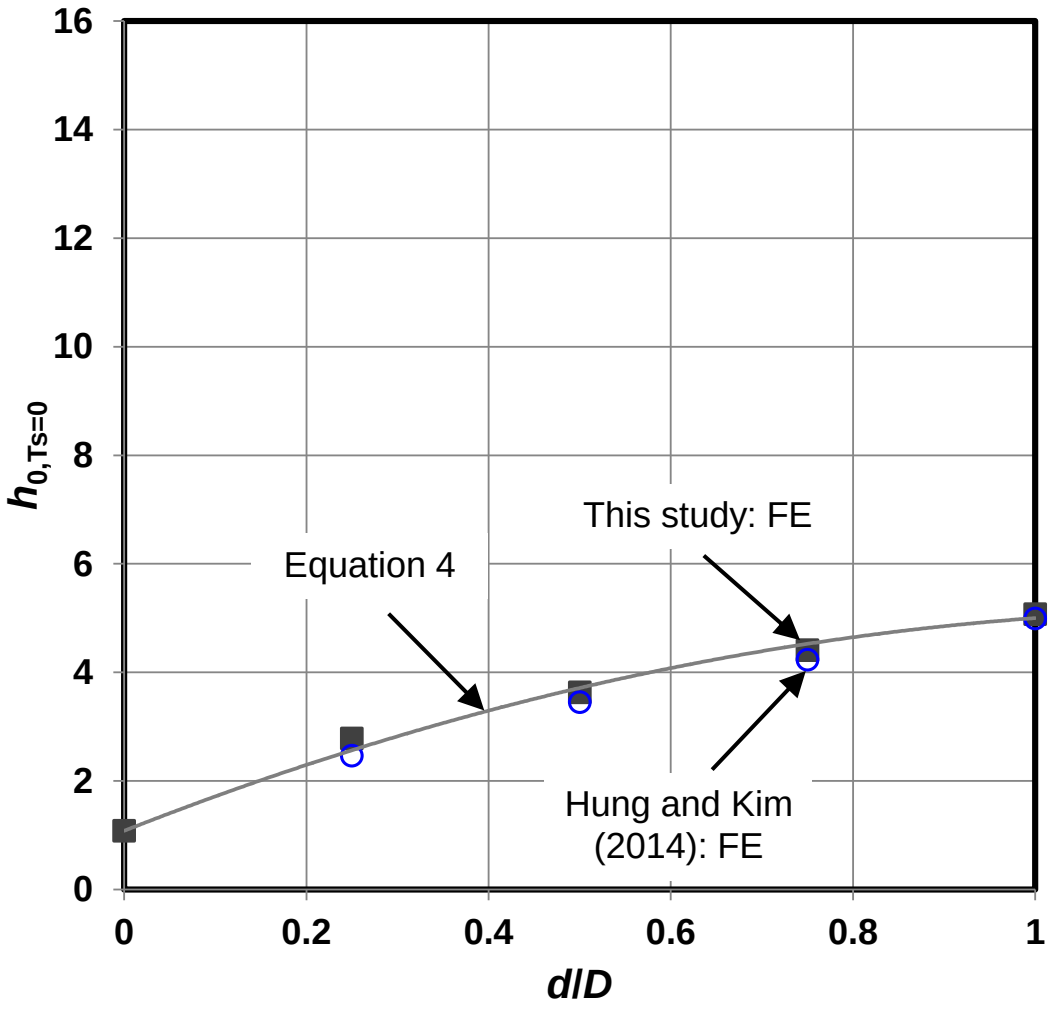

745

746 (a) Ultimate uniaxial horizontal load in clay (T_s/D = 0, κ_c = 3)

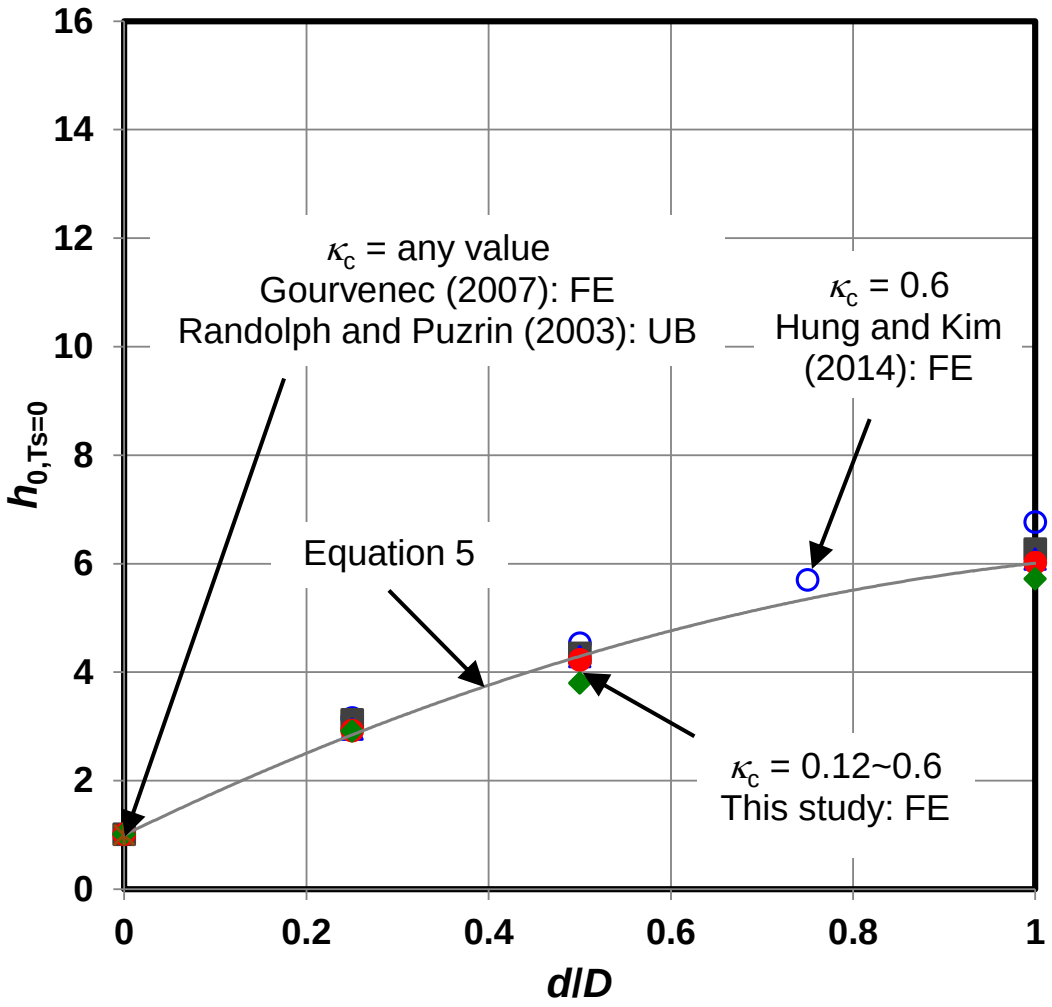

747

748 (b) Ultimate uniaxial horizontal load in clay (T_s/D = 0, κ_c = 0.12~0.6)

749

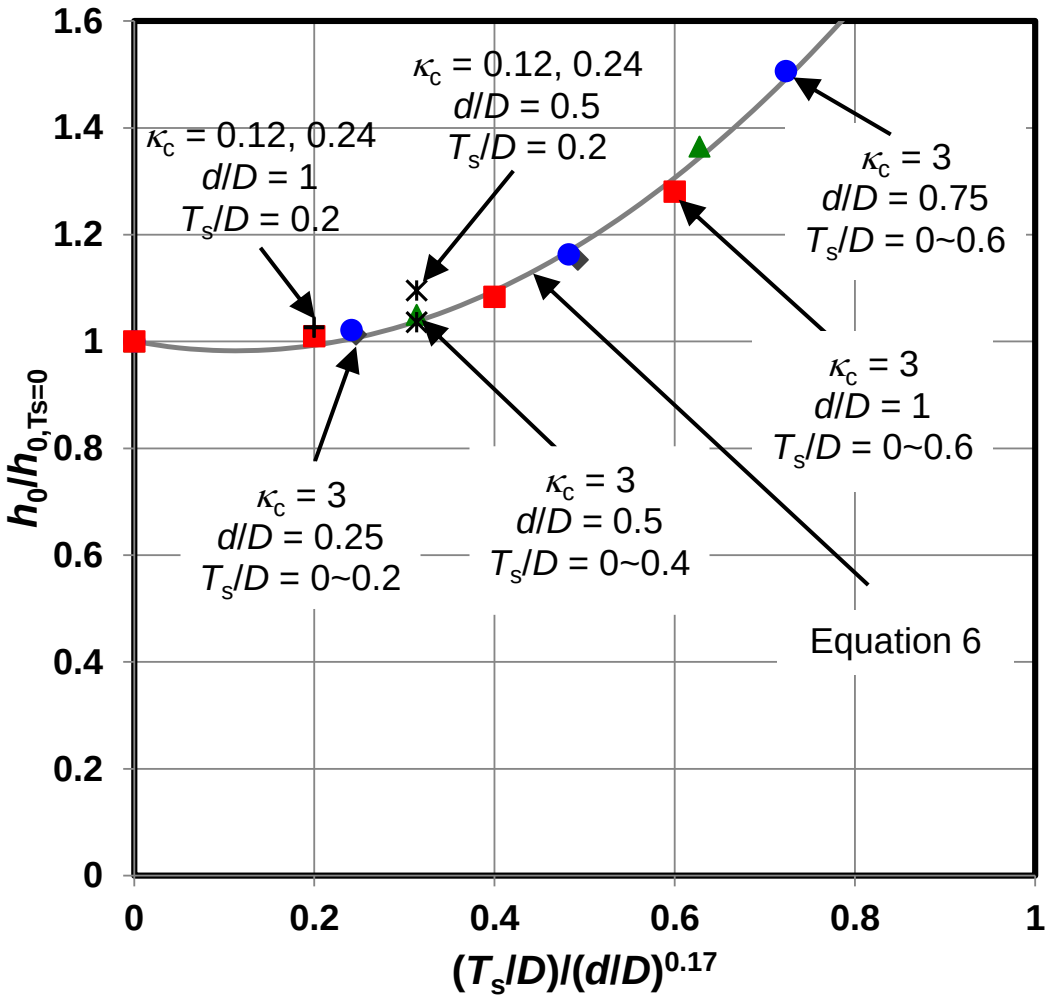

(c) Normalised ultimate uniaxial horizontal load in sand-over-clay (κ_c = 0.12~3)

Figure 6 Skirted foundations under uniaxial horizontal loading

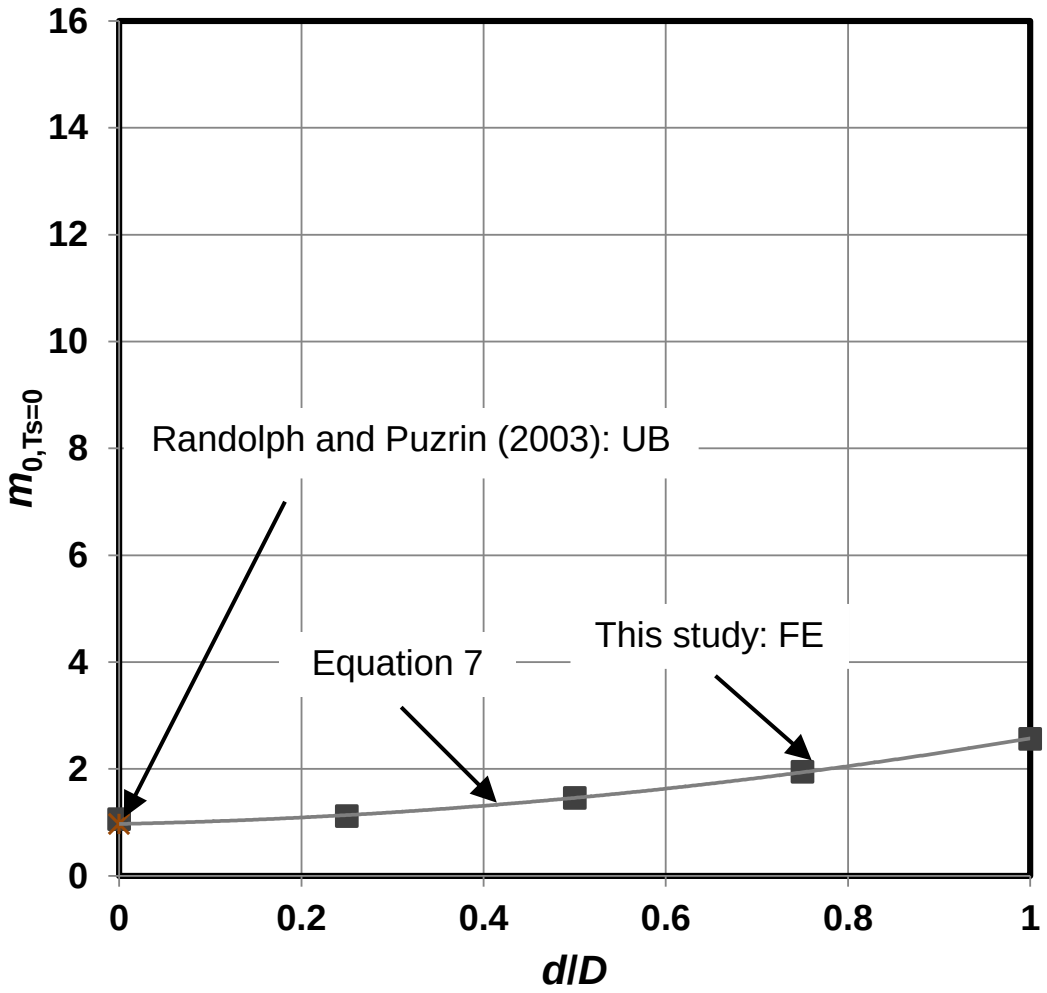

(a) Ultimate uniaxial moment load in clay (T_s/D = 0, κ_c = 3)

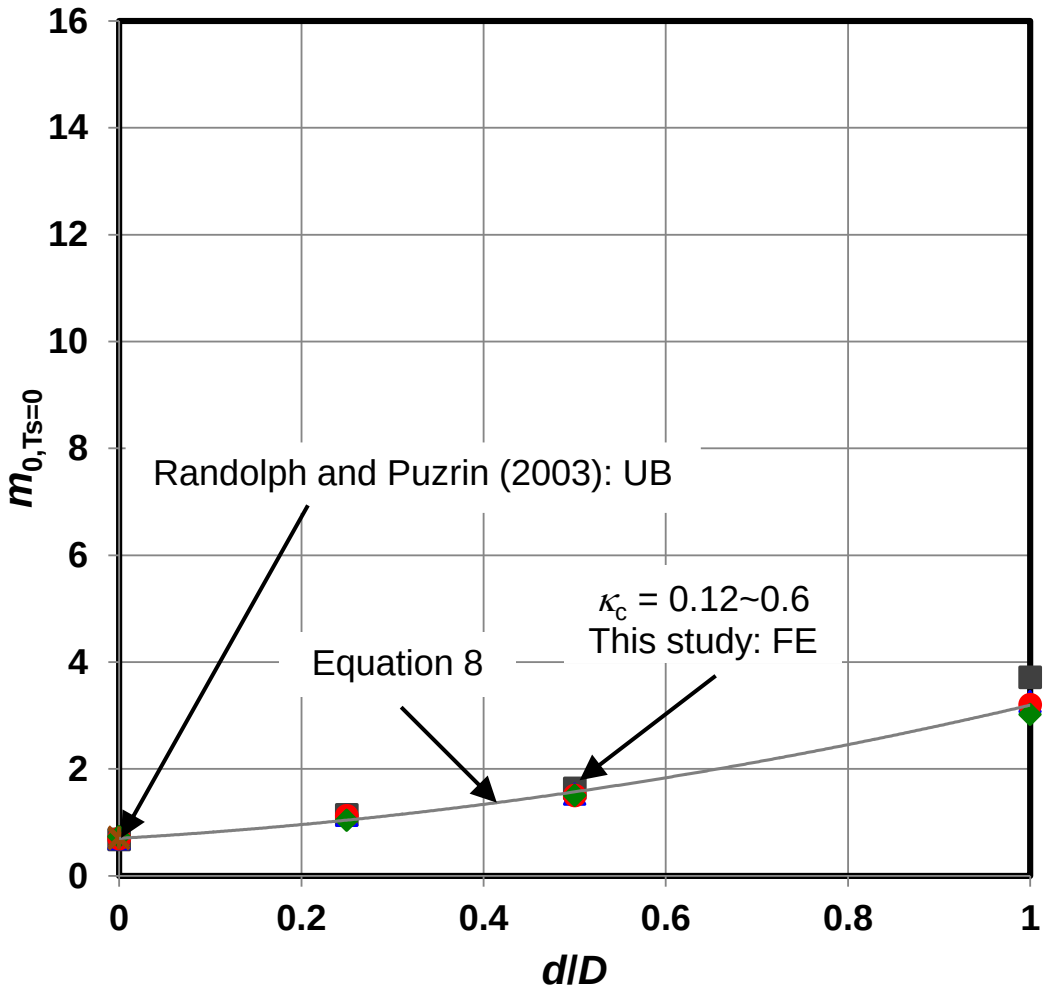

759

760 (b) Ultimate uniaxial moment load in clay (T_s/D = 0, κ_c = 0.12~0.6)

761

762

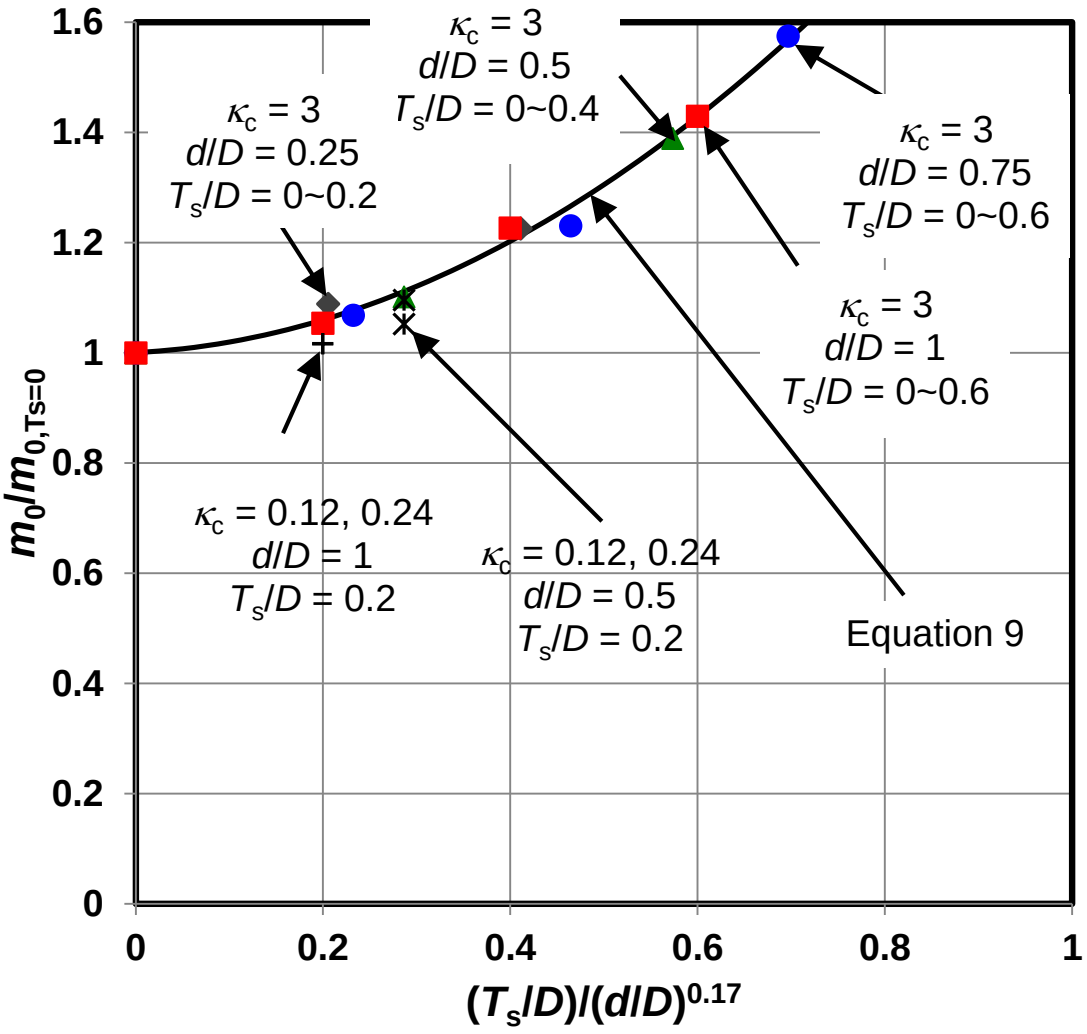

763

764 (c) Normalised ultimate uniaxial moment load in sand-over-clay (κ_c = 0.12~3)

765

766 **Figure 7 Skirted foundations under uniaxial moment loading**

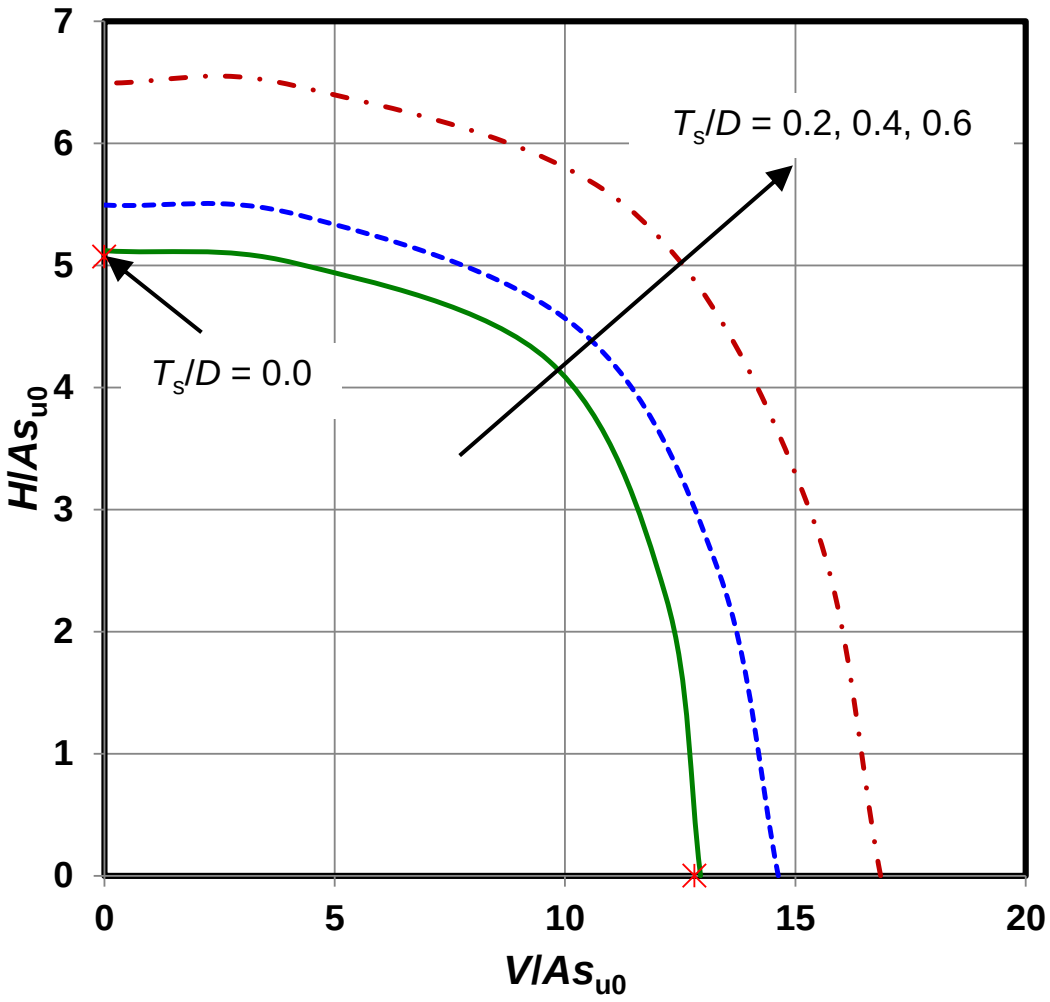

767

768 (a) d/D = 1.0

769

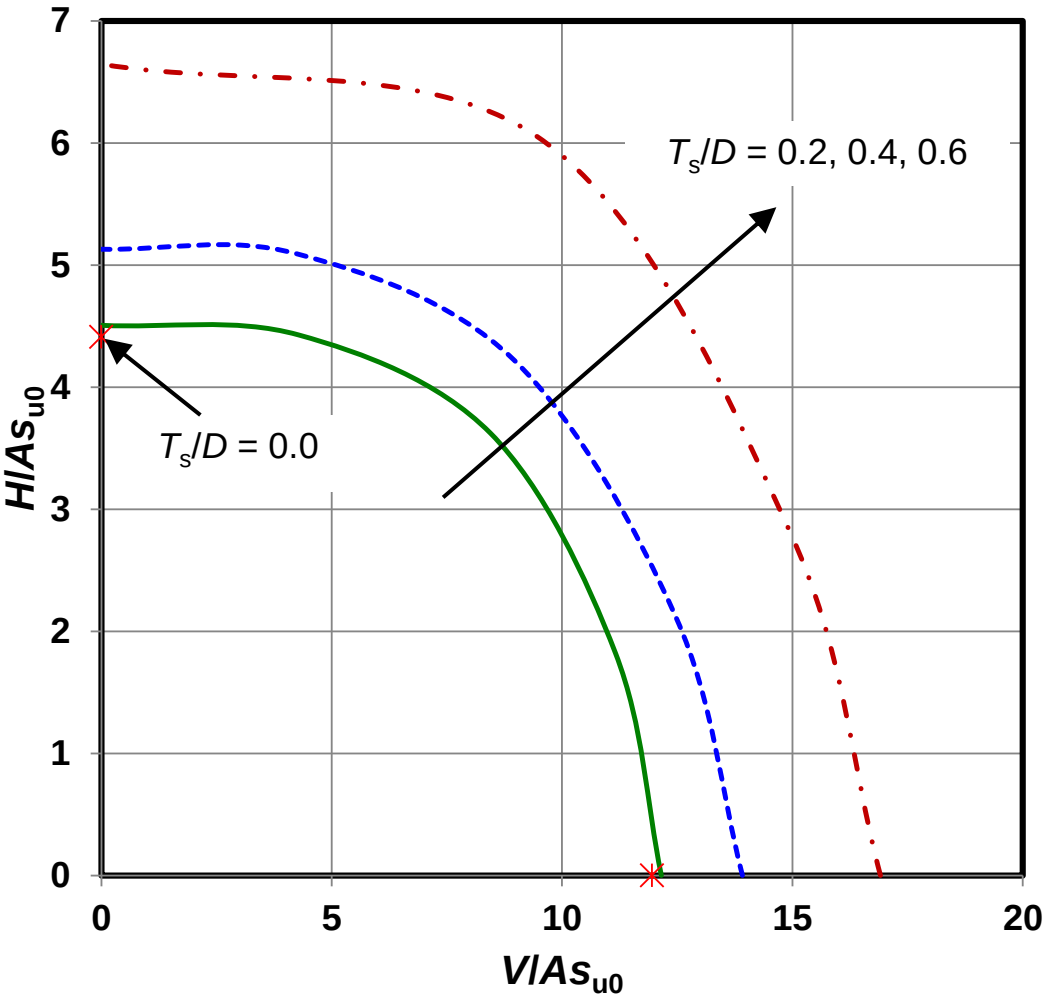

(b) $d/D = 0.75$

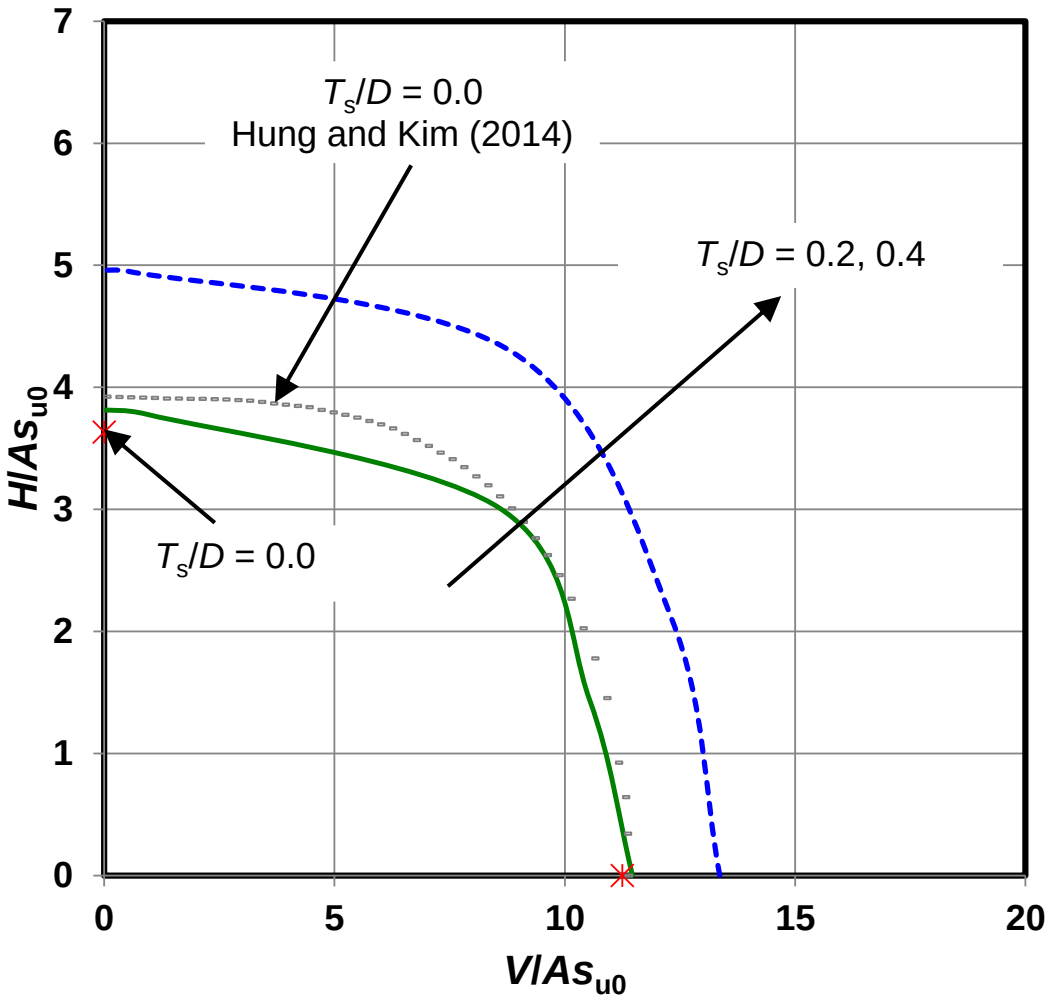

773
774

(c) d/D = 0.5

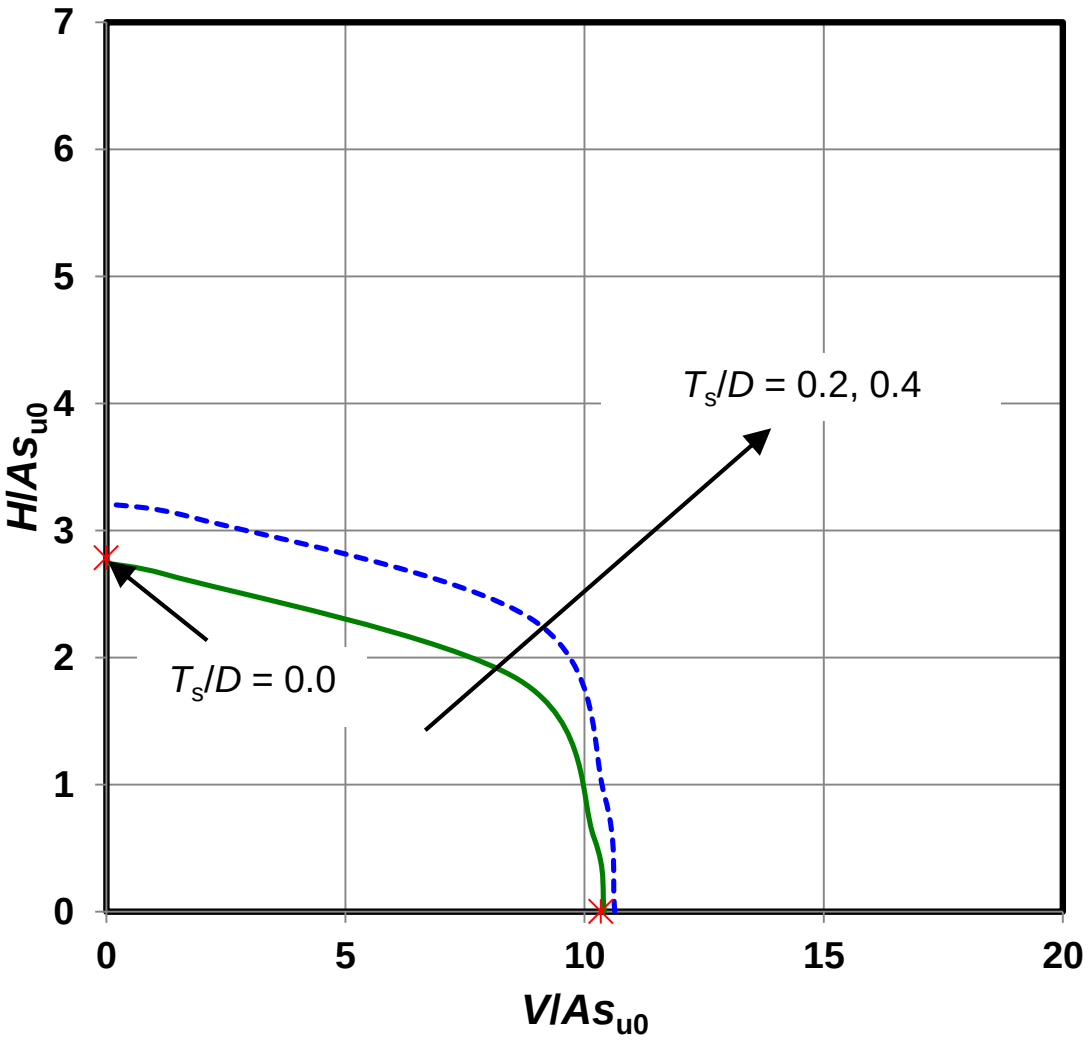

(d) $d/D = 0.25$

Figure 8 Failure envelopes in *V*-*H* space

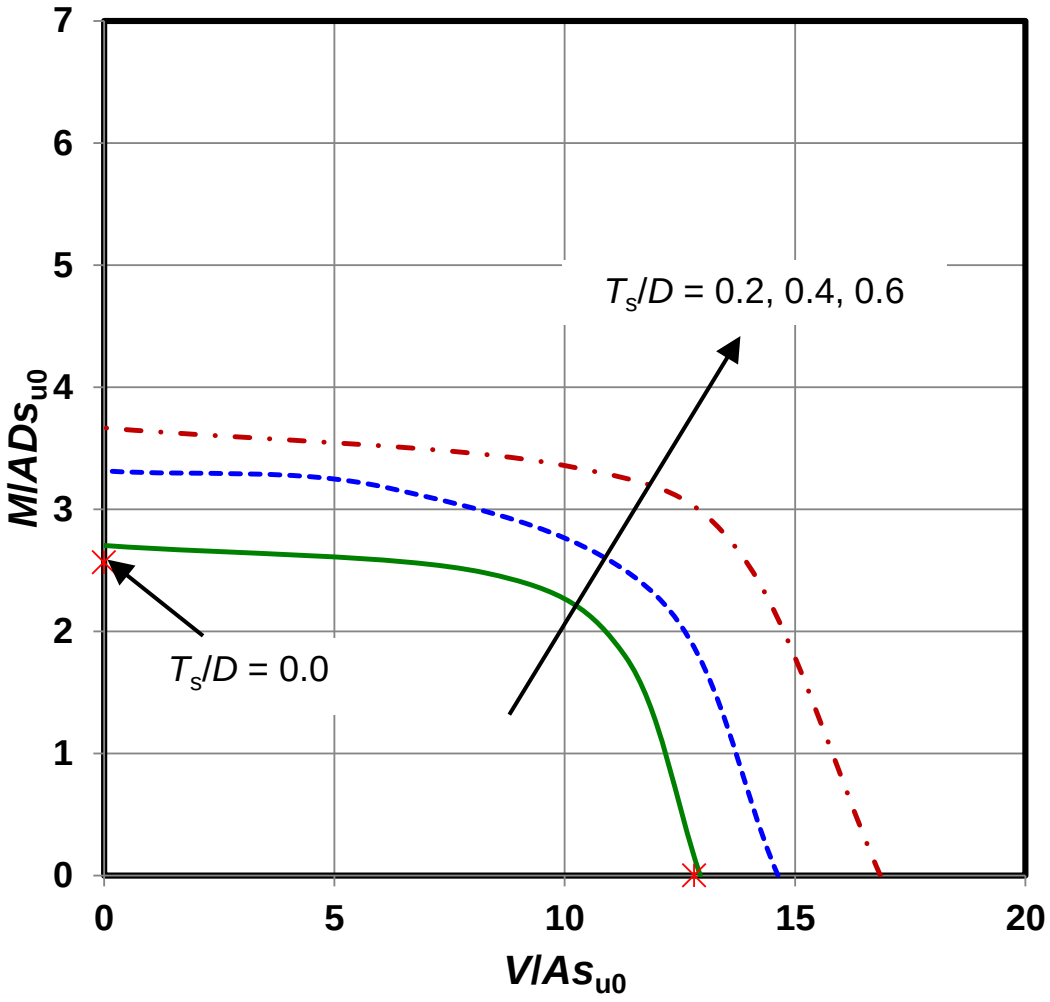

781
782 (a) d/D = 1.0
783

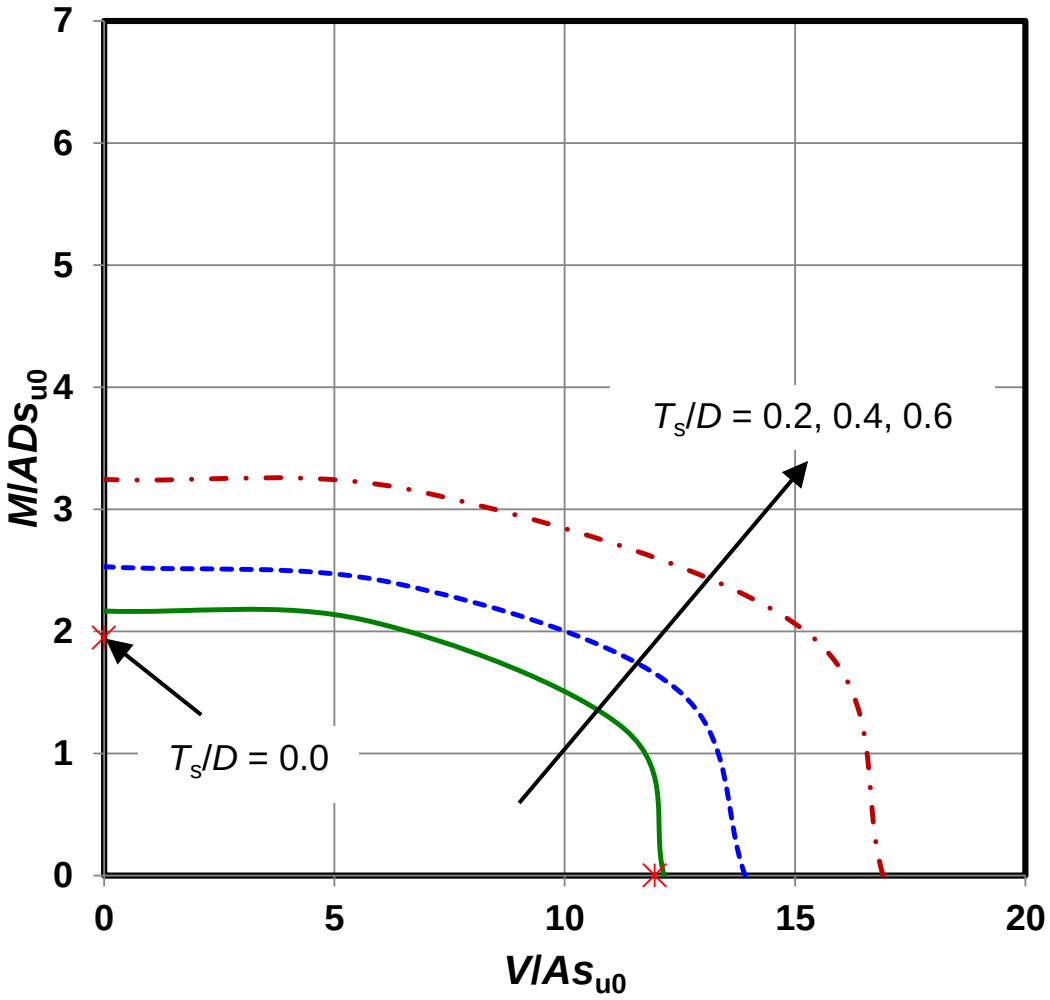

(b) d/D = 0.75

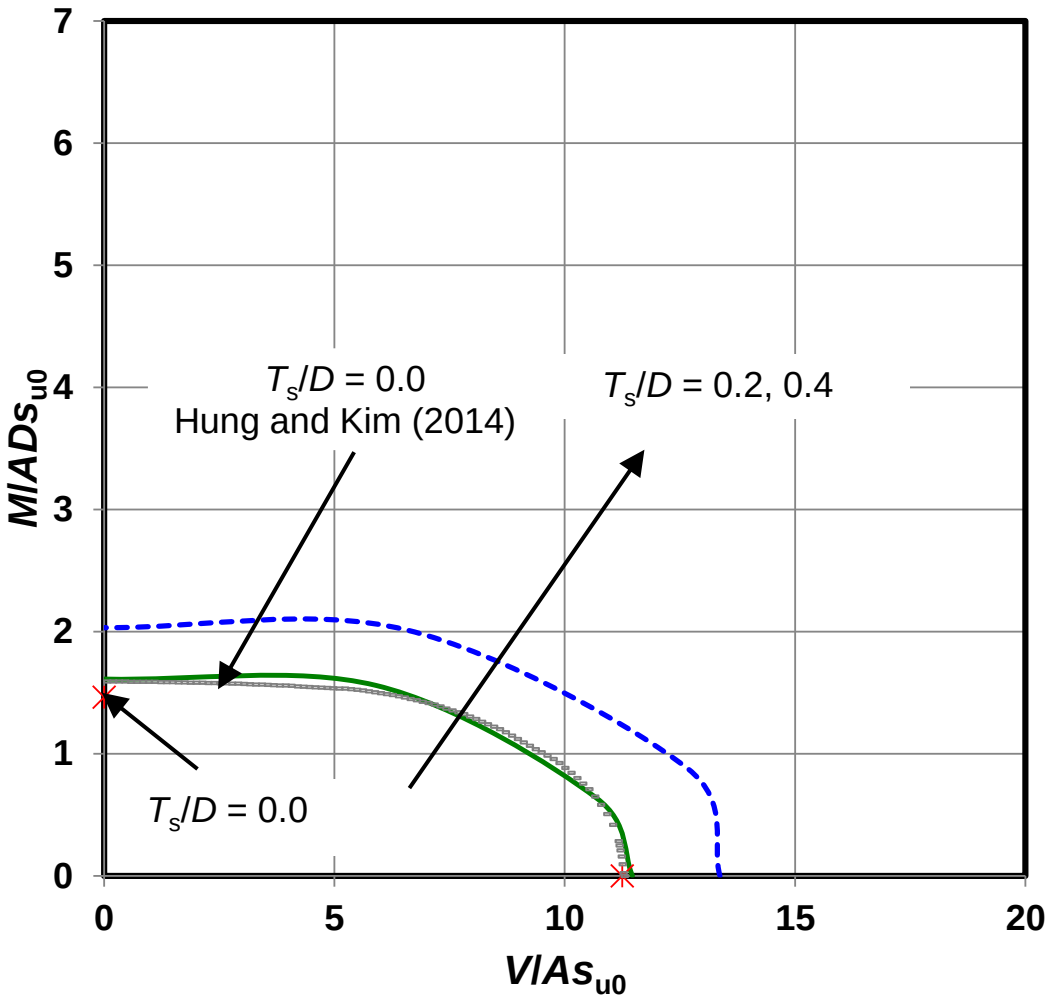

787
788 (c) d/D = 0.5
789

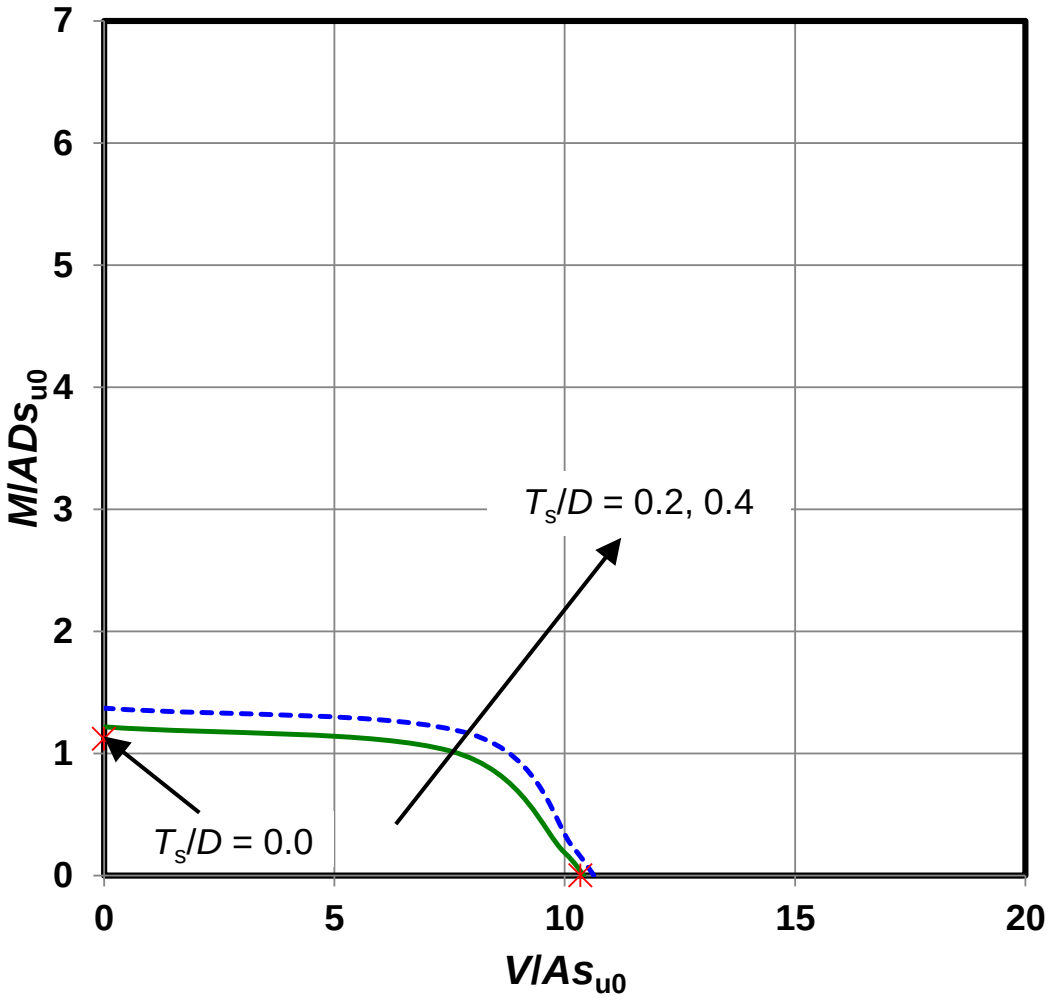

(d) $d/D = 0.25$

Figure 9 Failure envelopes in *V*-*M* space

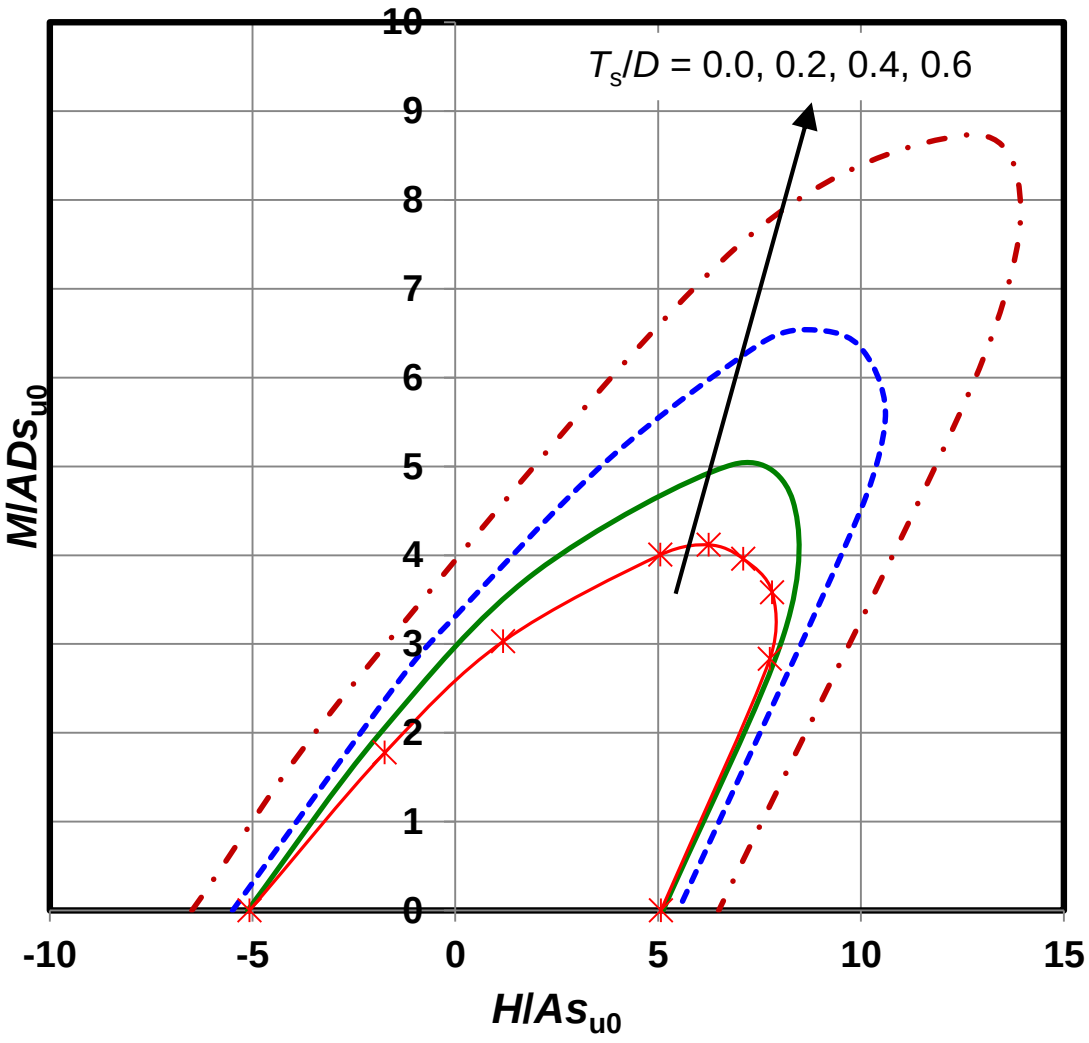

(a) d/D = 1.0

799

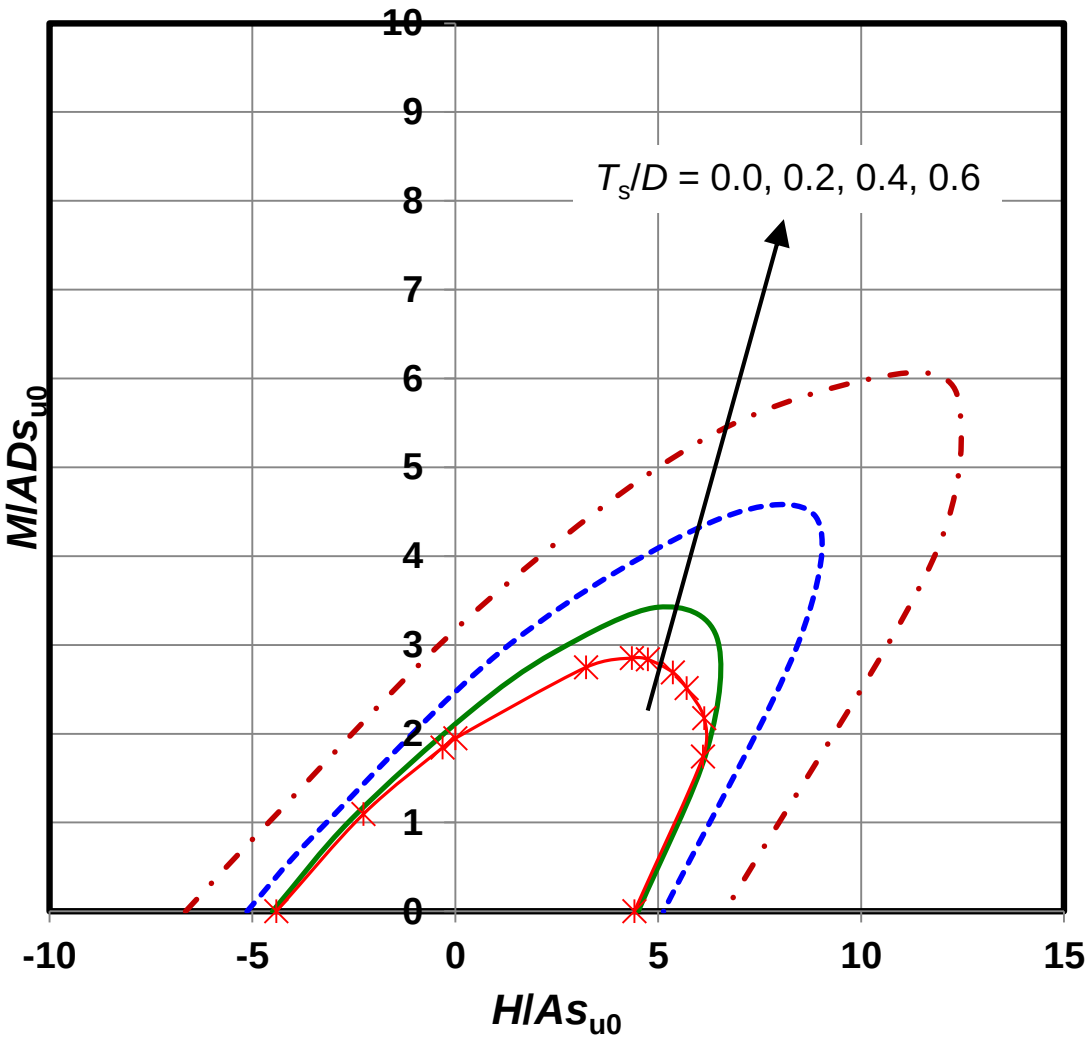

800
801 (b) d/D = 0.75
802

803

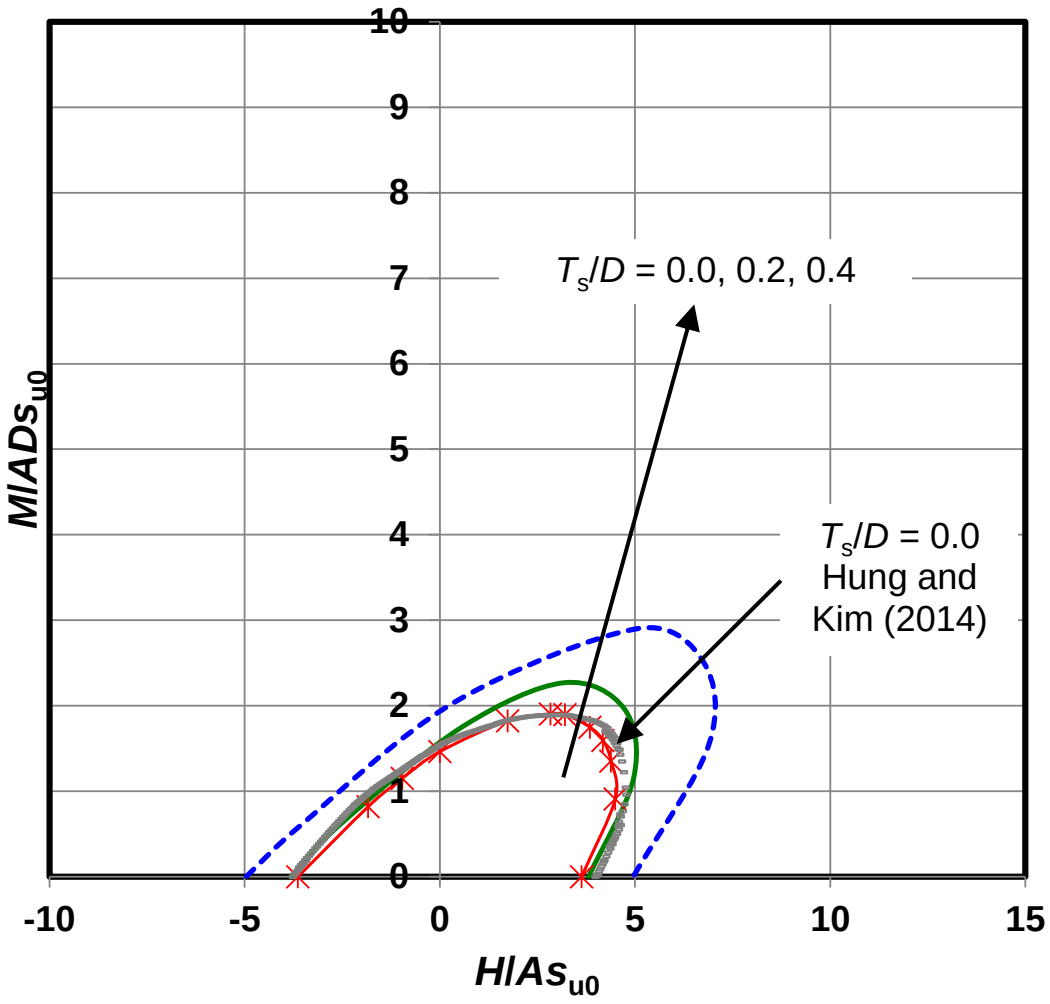

804
805 (c) $d/D = 0.5$
806

807

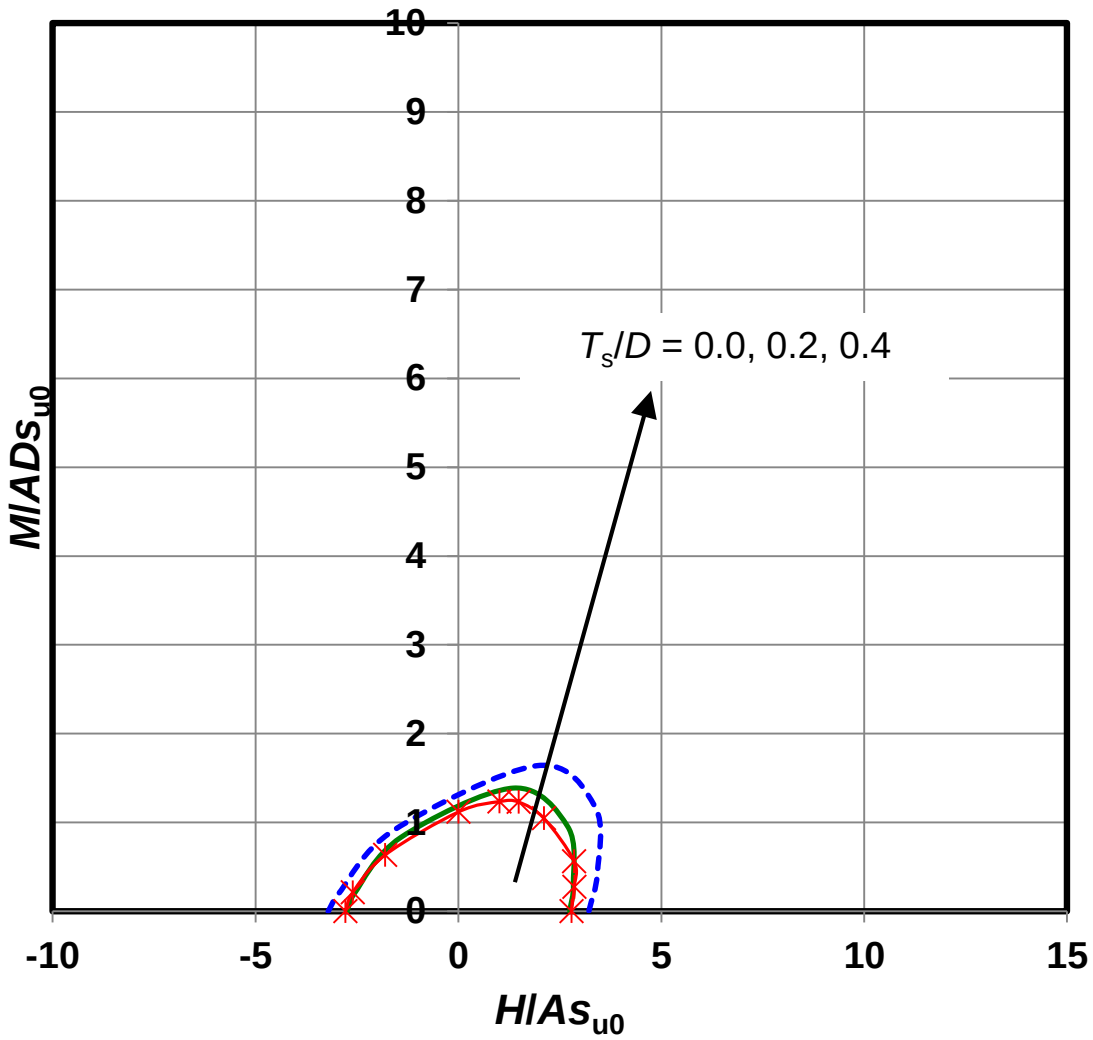

808
809 (d) d/D = 0.25

810
811 **Figure 10 Failure envelopes in *H*-*M* space**
812

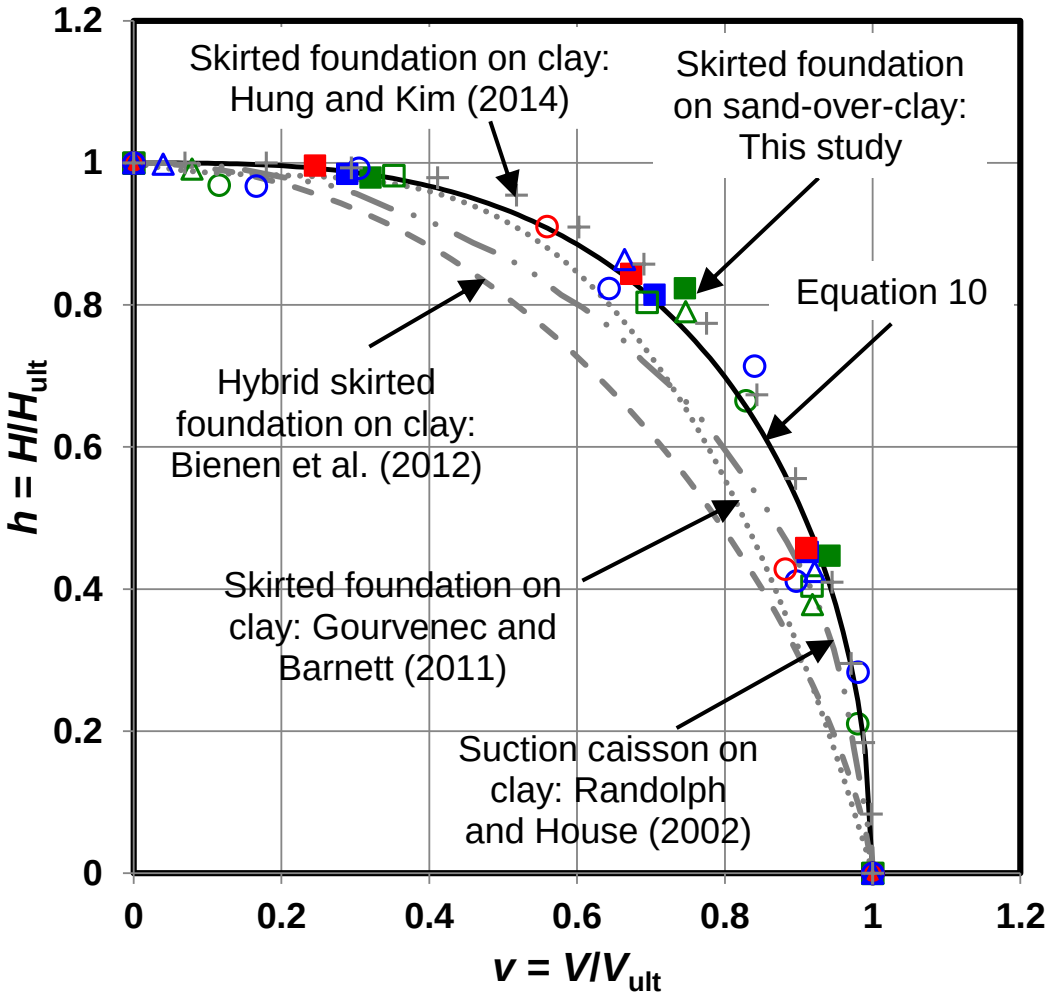
Skirted foundation on clay: Hung and Kim (2014)
Skirted foundation on sand-over-clay: This study
Equation 10
Hybrid skirted foundation on clay: Bienen et al. (2012)
Skirted foundation on clay: Gourvenec and Barnett (2011)
Suction caisson on clay: Randolph and House (2002)
h = H/H_ult
v = V/V_ult
0
0.2
0.4
0.6
0.8
1
1.2

(a) *v*-*h* space

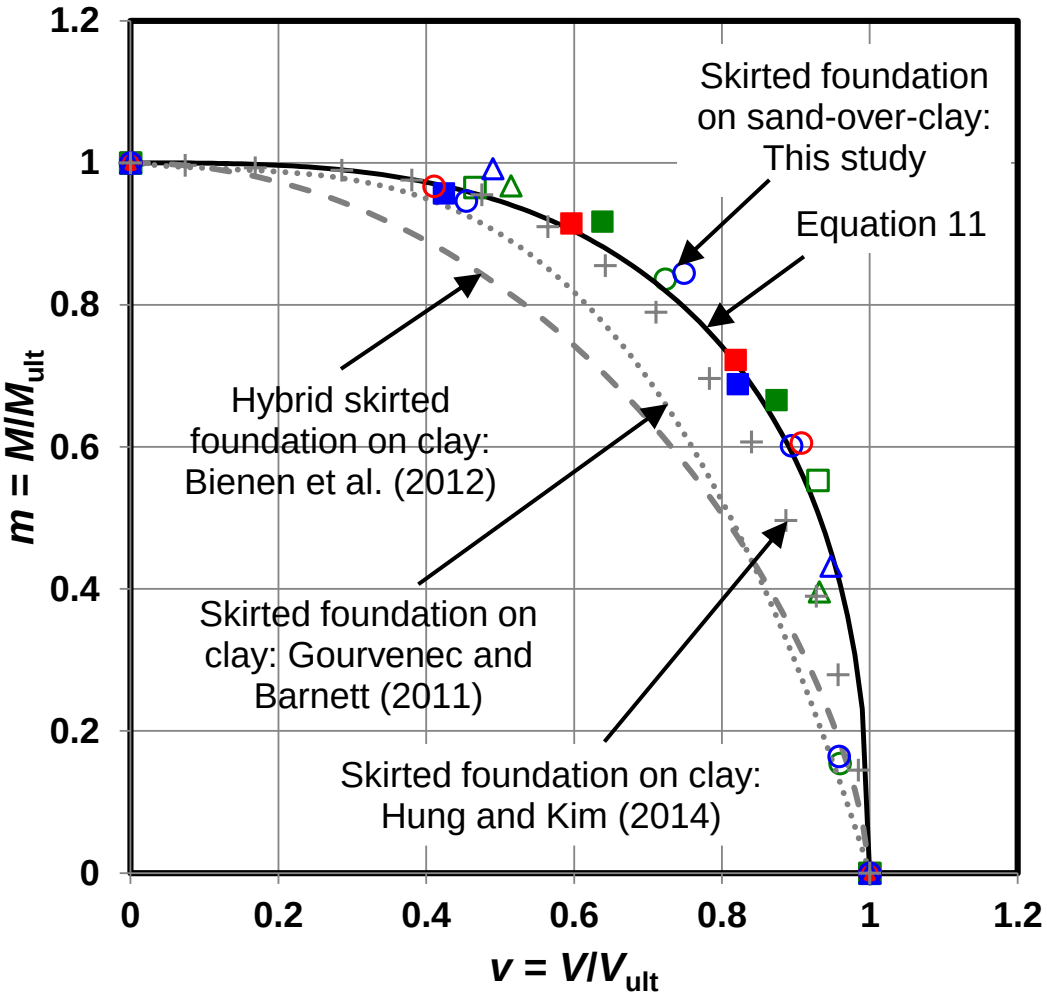

(b) *v*-*m* space

Figure 11 Normalised failure envelopes

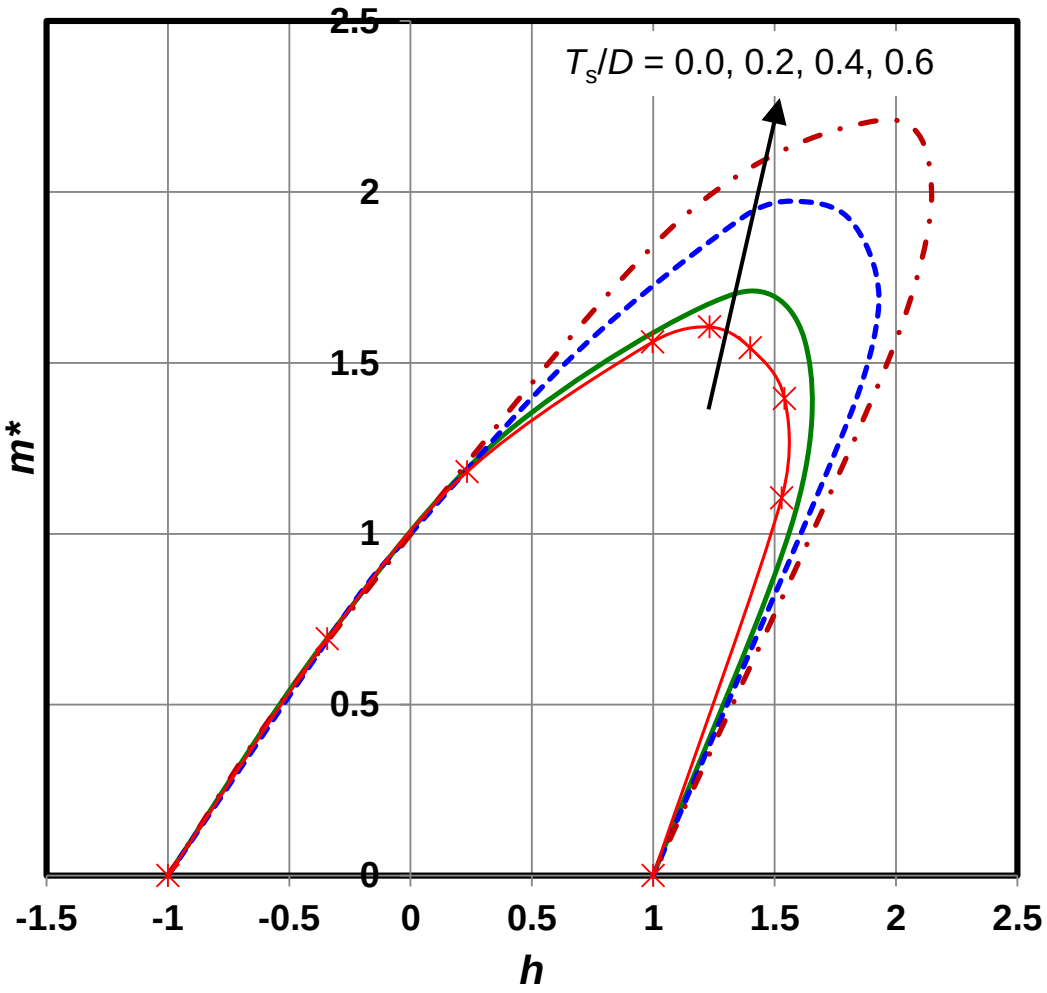

(a) d/D = 1.0

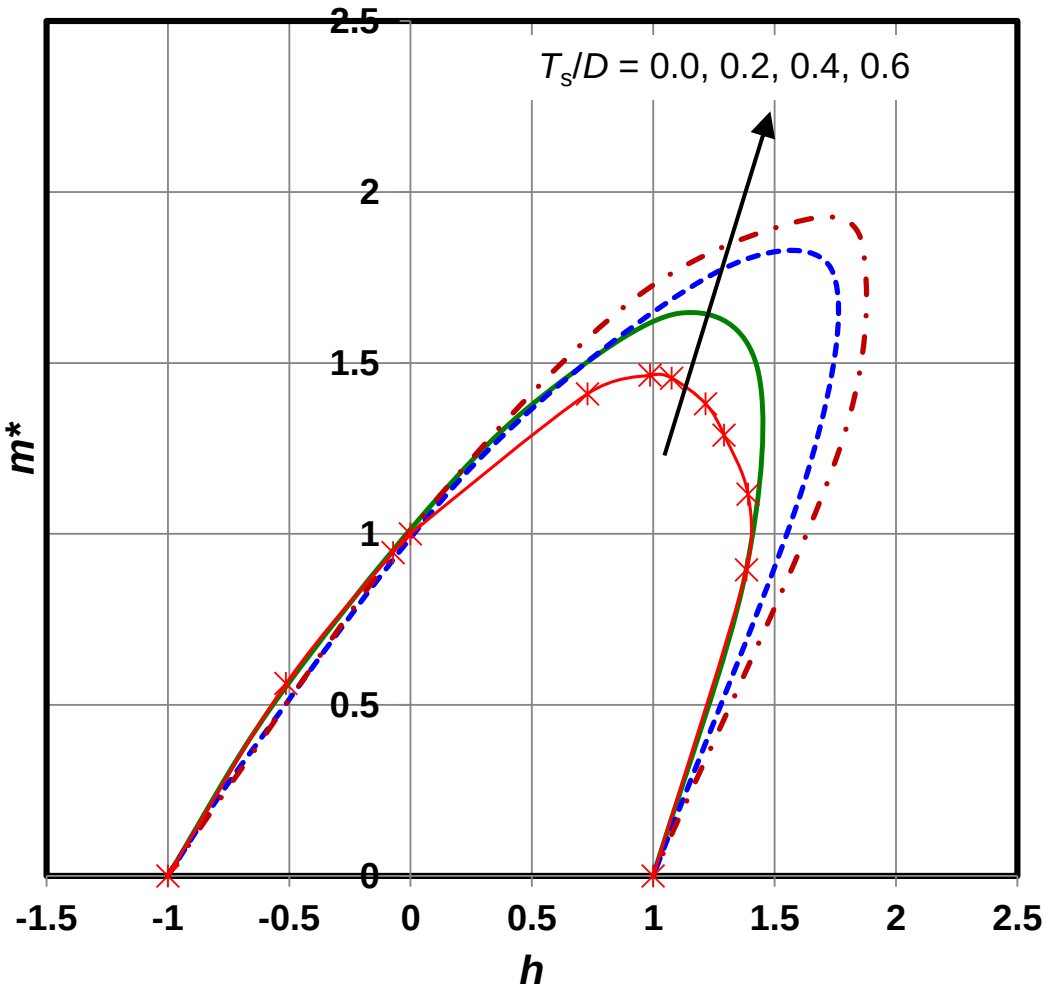

(b) d/D = 0.75

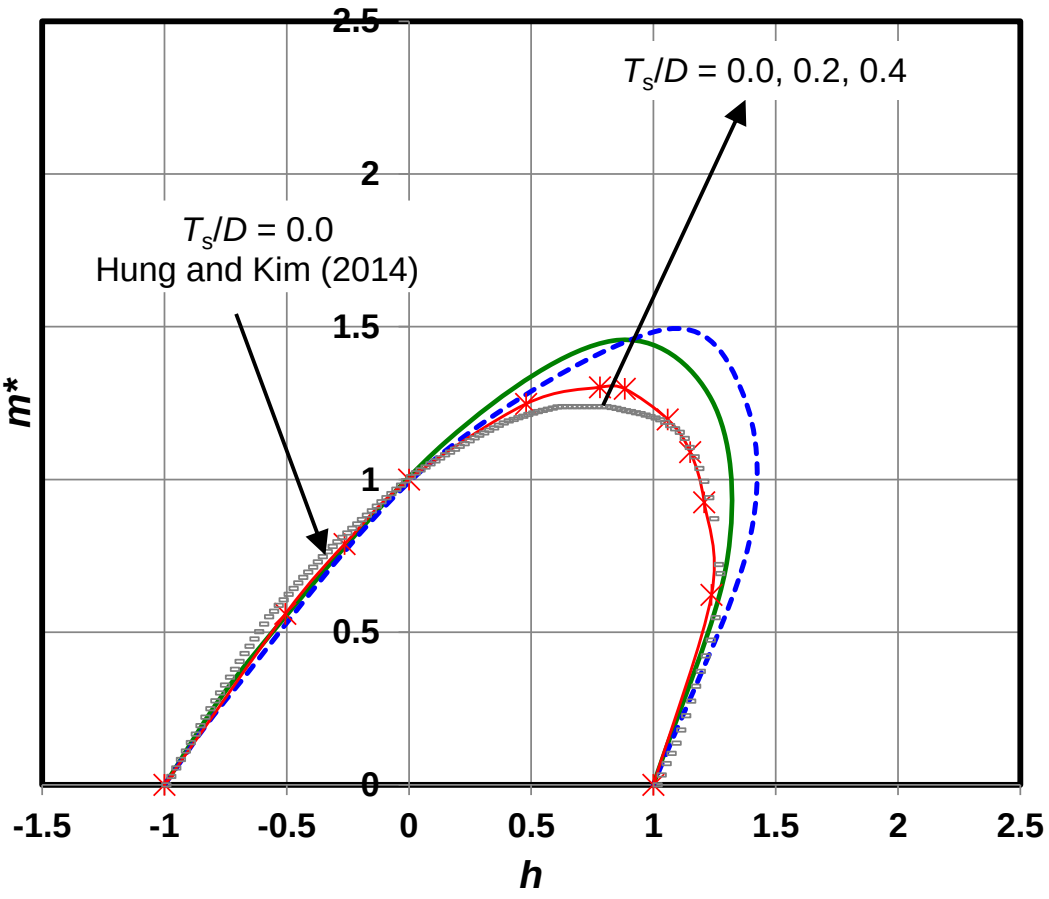
2.5
2
1.5
1
0.5
0
-1.5
-1
-0.5
0
0.5
1
1.5
2
2.5
m*
h
T_s/D = 0.0, 0.2, 0.4
T_s/D = 0.0
Hung and Kim (2014)

(c) d/D = 0.5

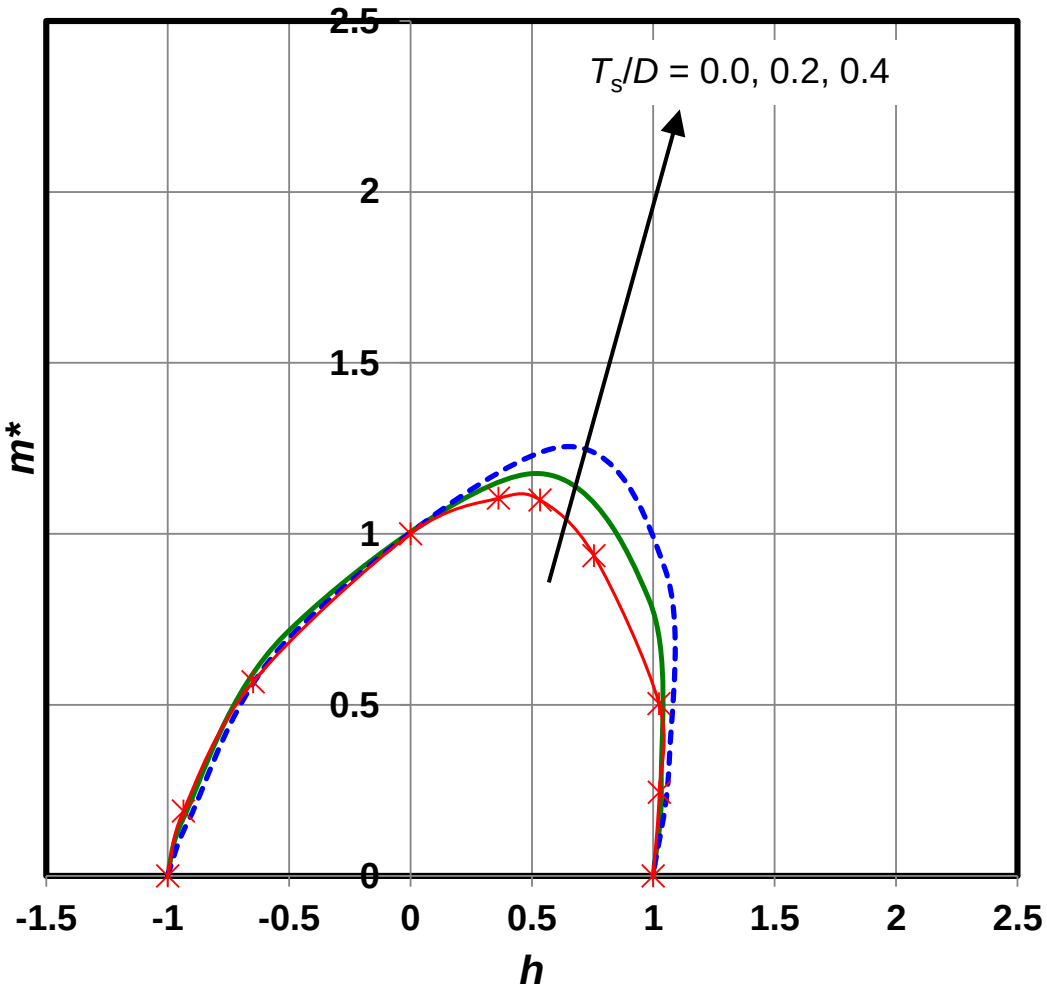

(d) d/D = 0.25

Figure 12 Normalised failure envelopes in *h*-*m* space (v = 0)

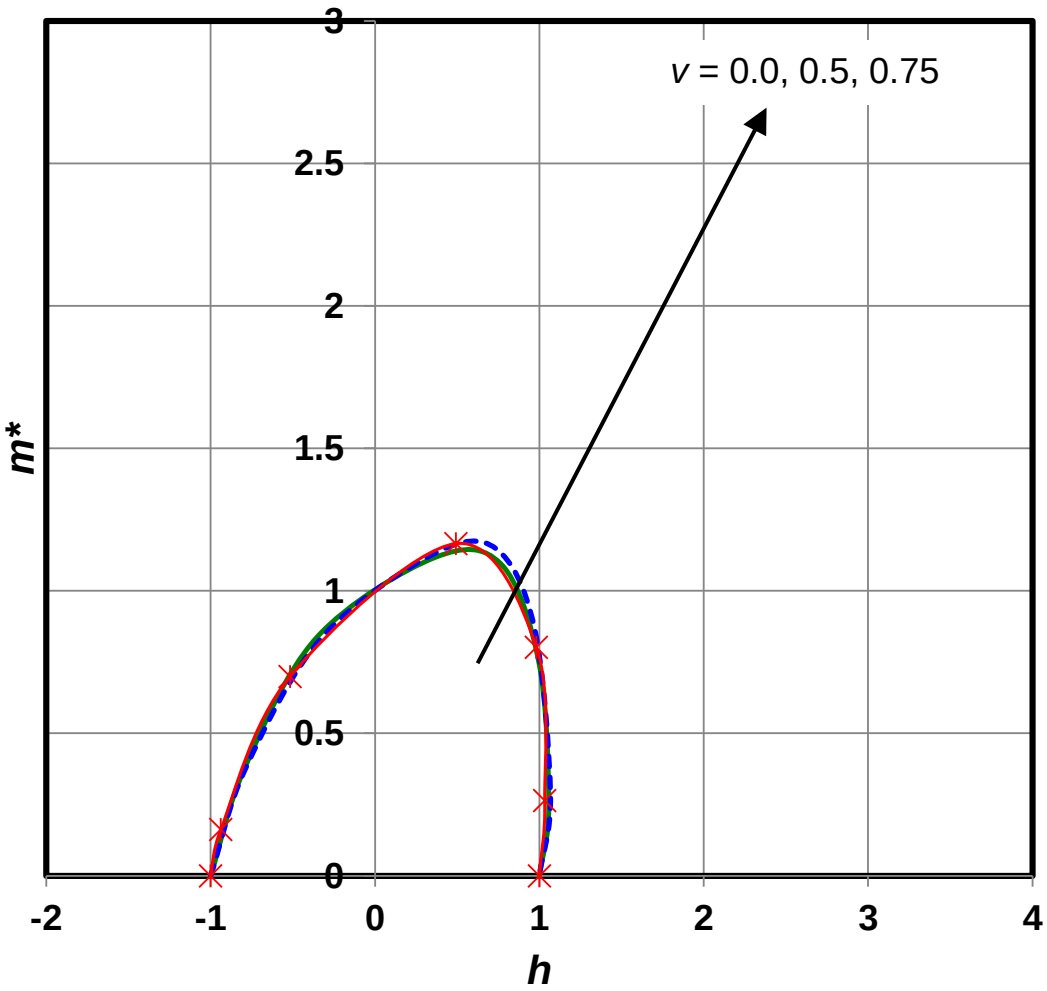

(a) T_s/D = 0.1

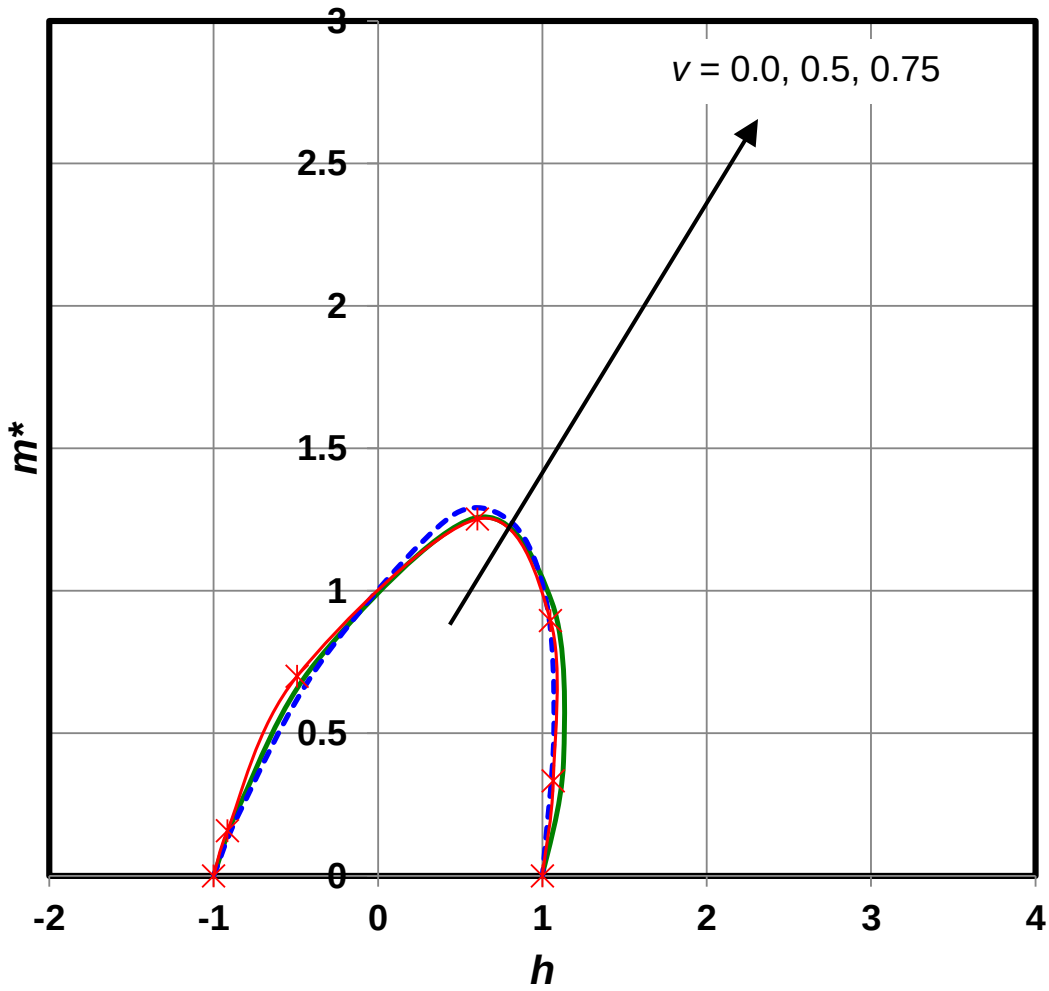

(b) T_s/D = 0.2

Figure 13 Effect of vertical mobilisation *v* on normalised failure envelopes in *h*-*m* space: *d*/*D* = 0.25

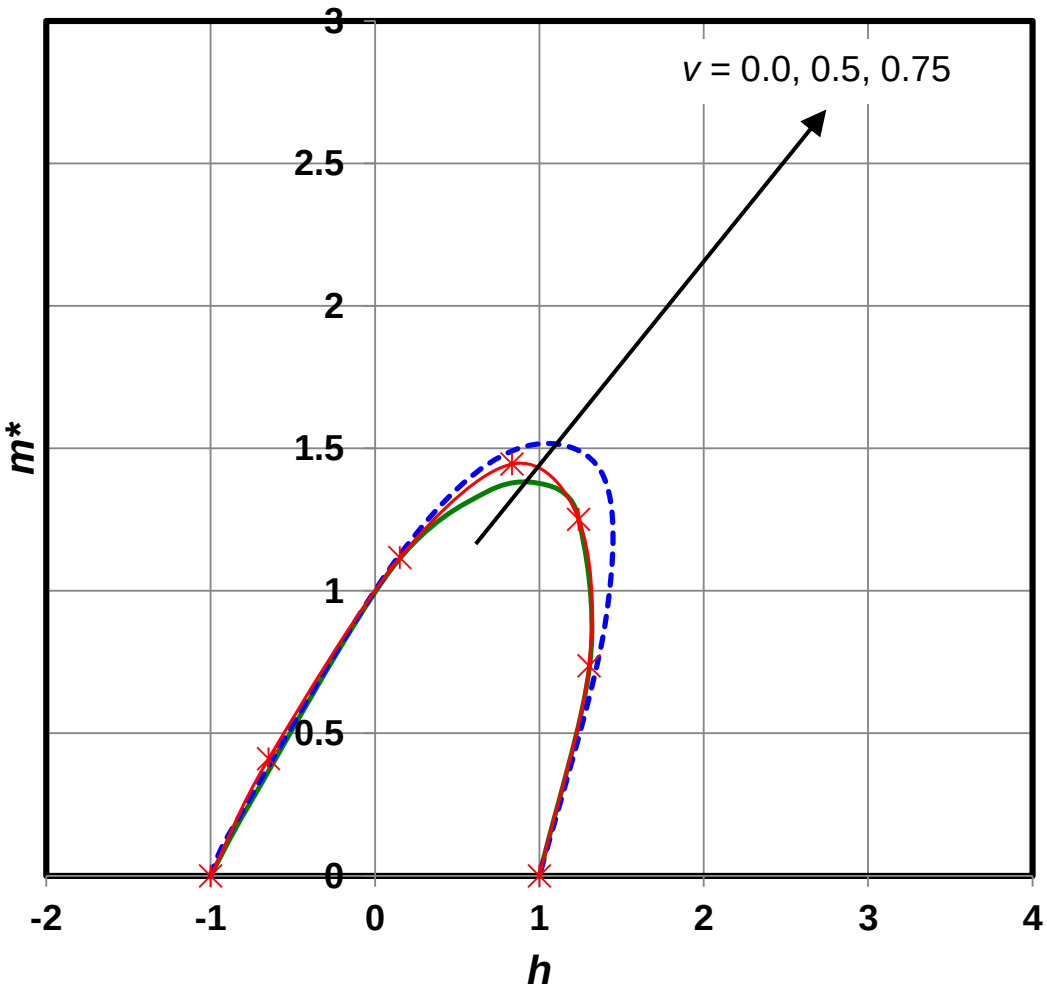

(a) T_s/D = 0.2

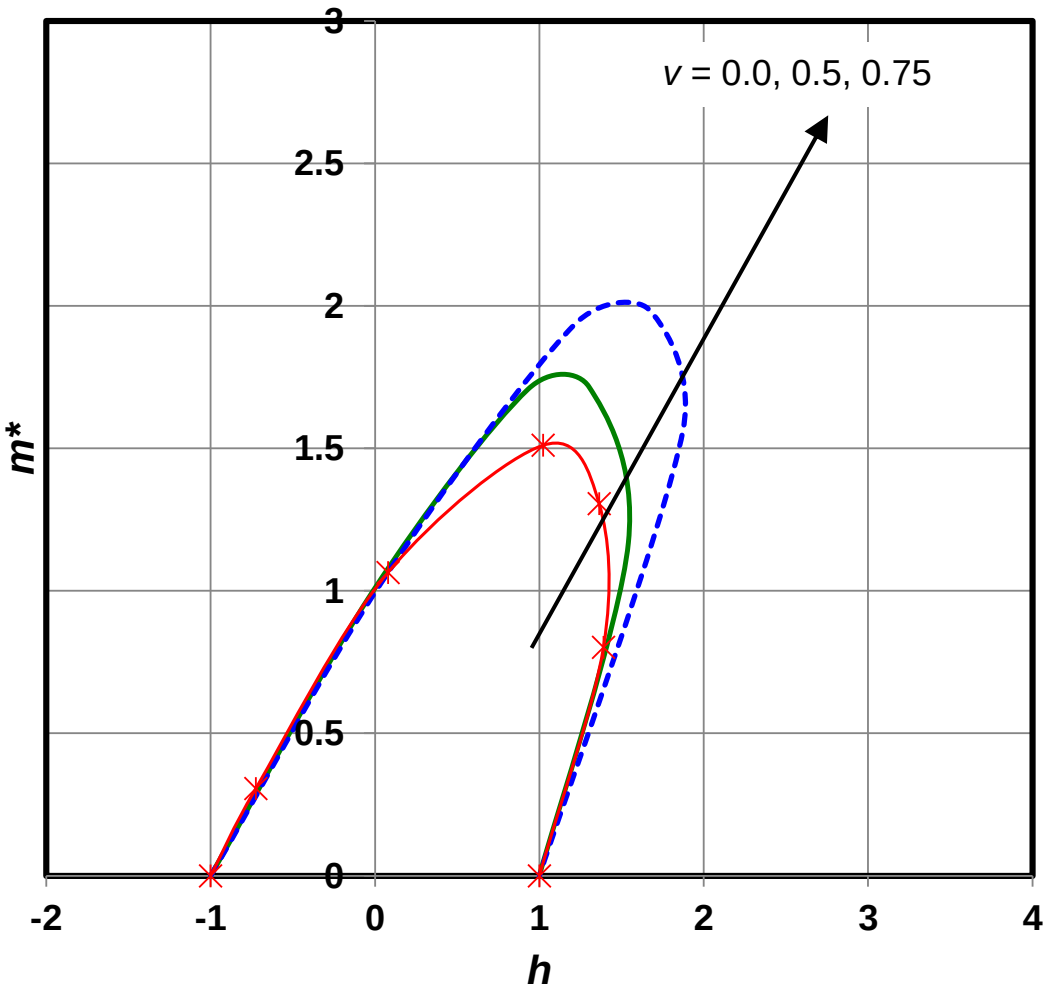

(b) T_s/D = 0.4

Figure 14 Effect of vertical mobilisation *v* on normalised failure envelopes in *h*-*m* space: *d*/*D* = 0.5

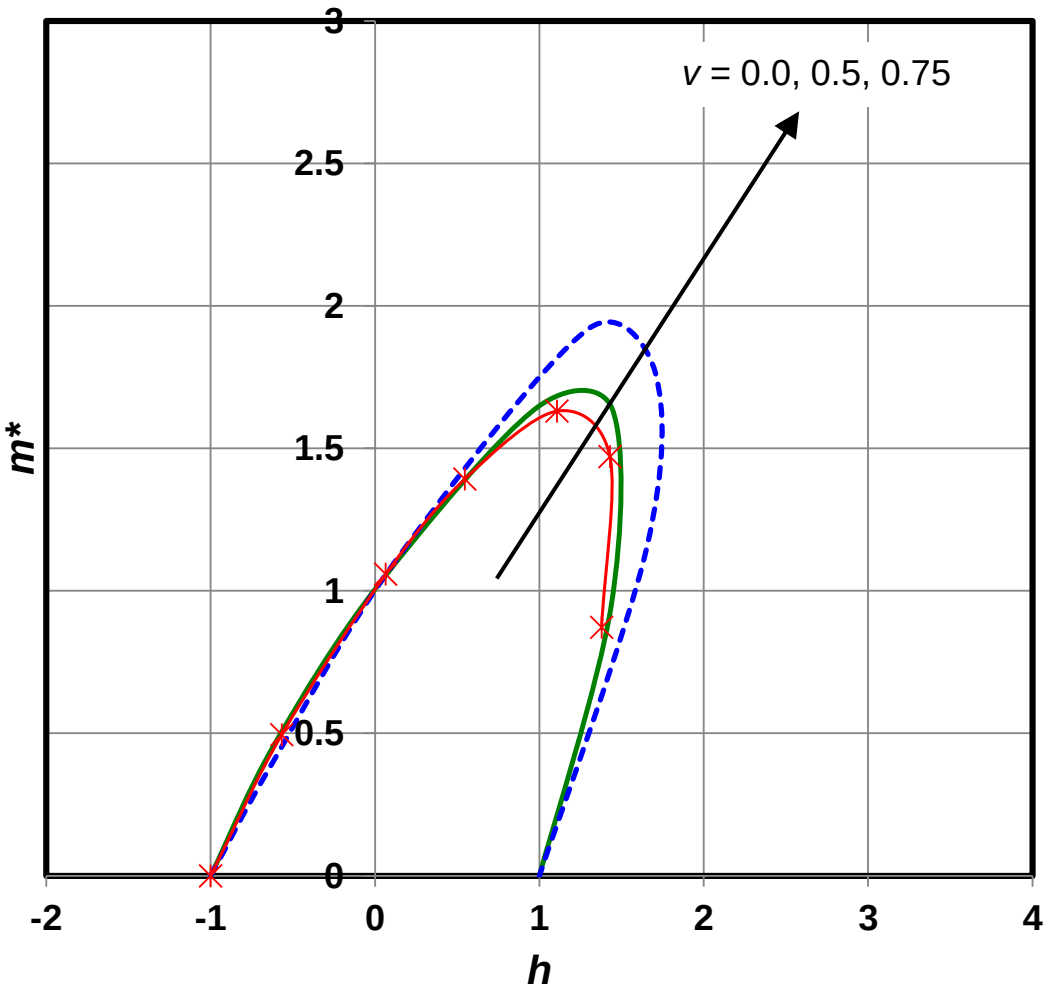

(a) T_s/D = 0.2

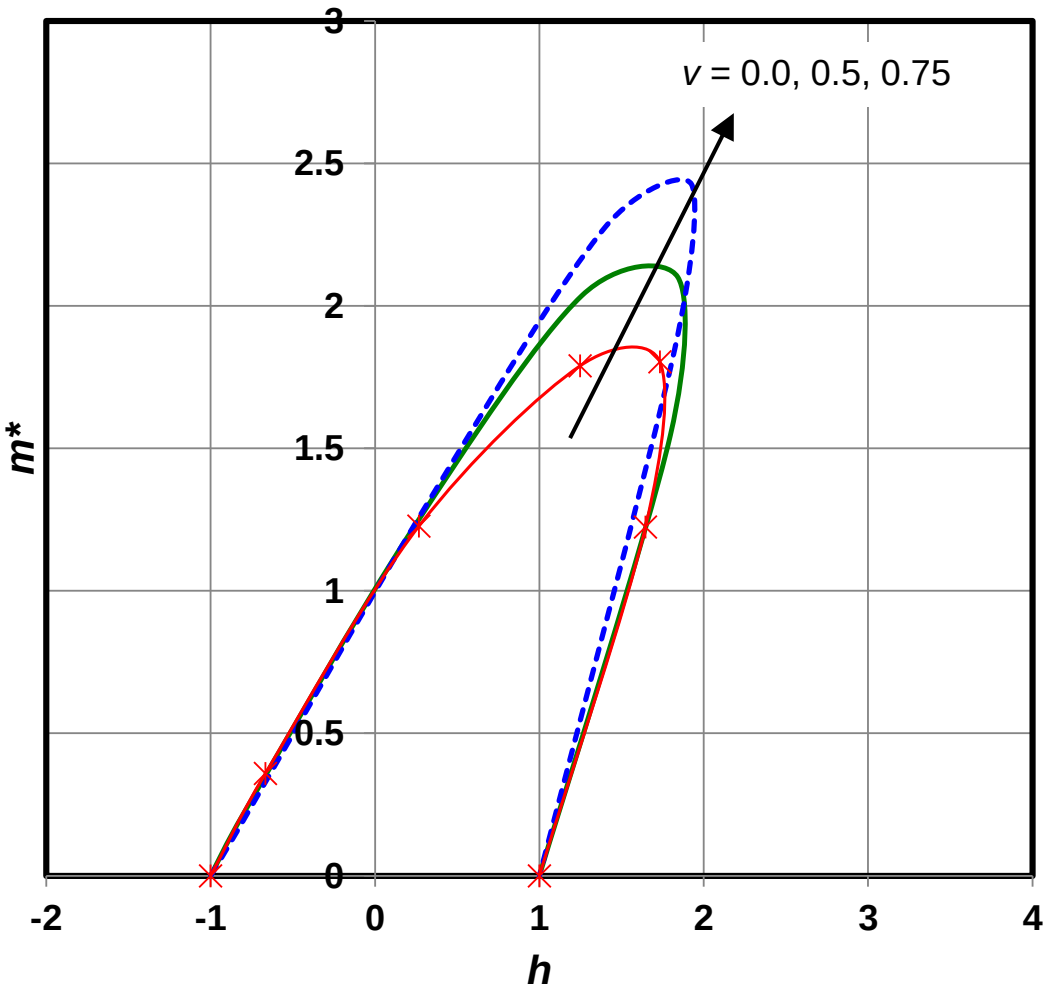

(b) T_s/D = 0.4

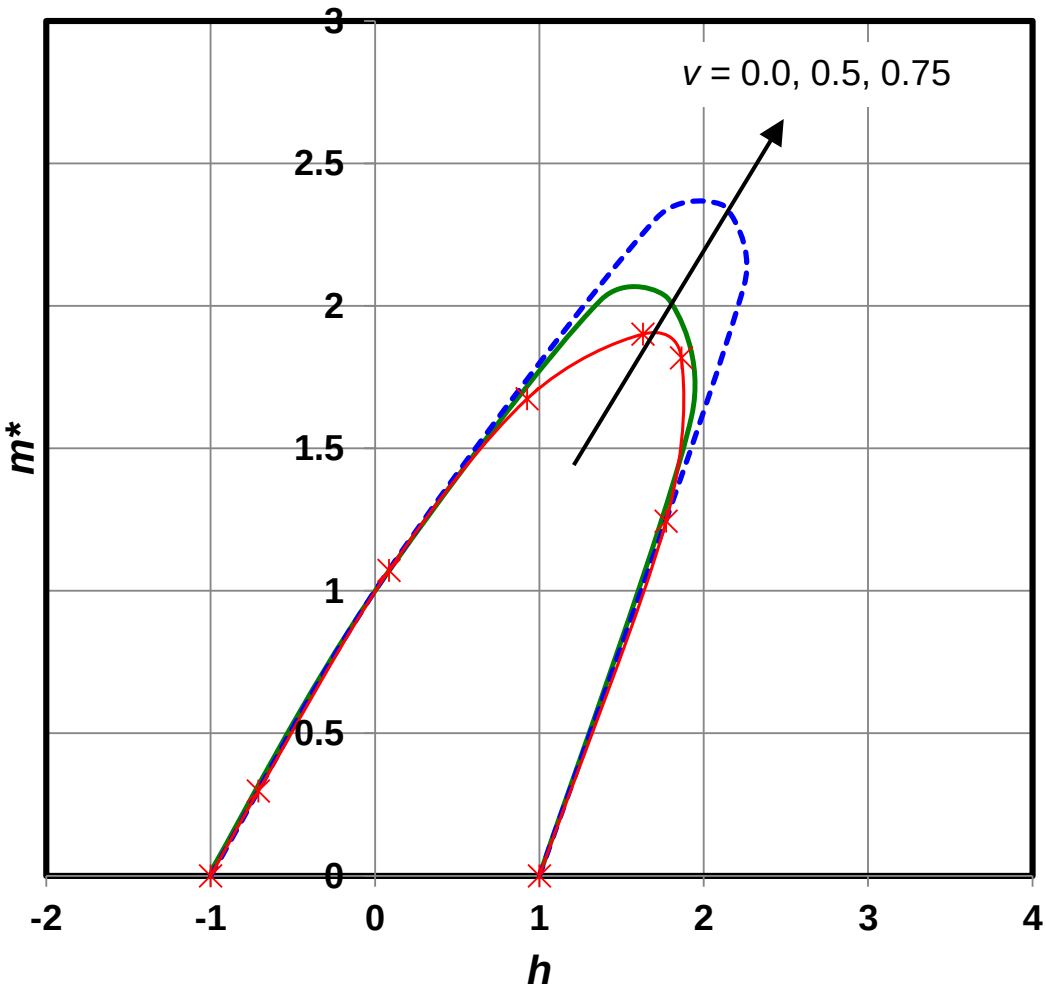

(c) T_s/D = 0.6

Figure 15 Effect of vertical mobilisation *v* on normalised failure envelopes in *h*-*m* space: *d*/*D* = 0.75

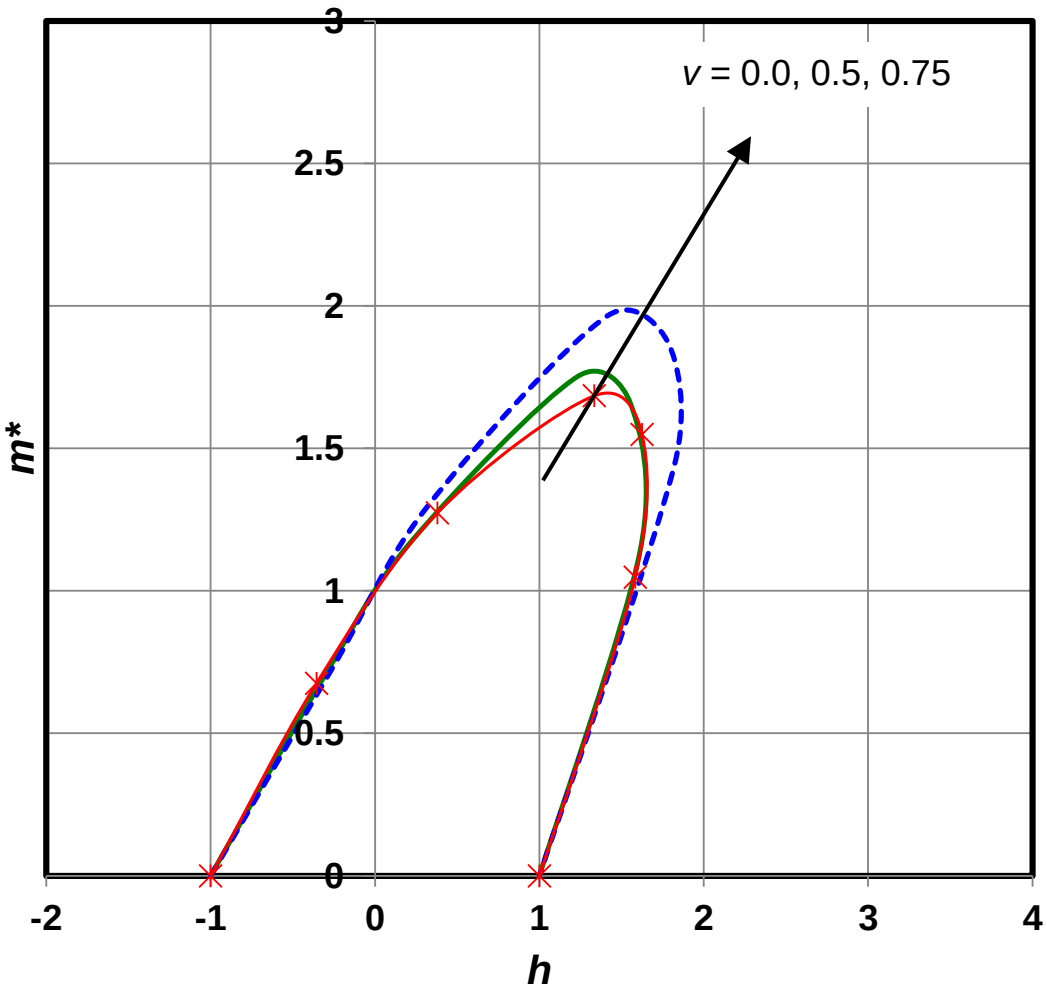

(a) T_s/D = 0.2

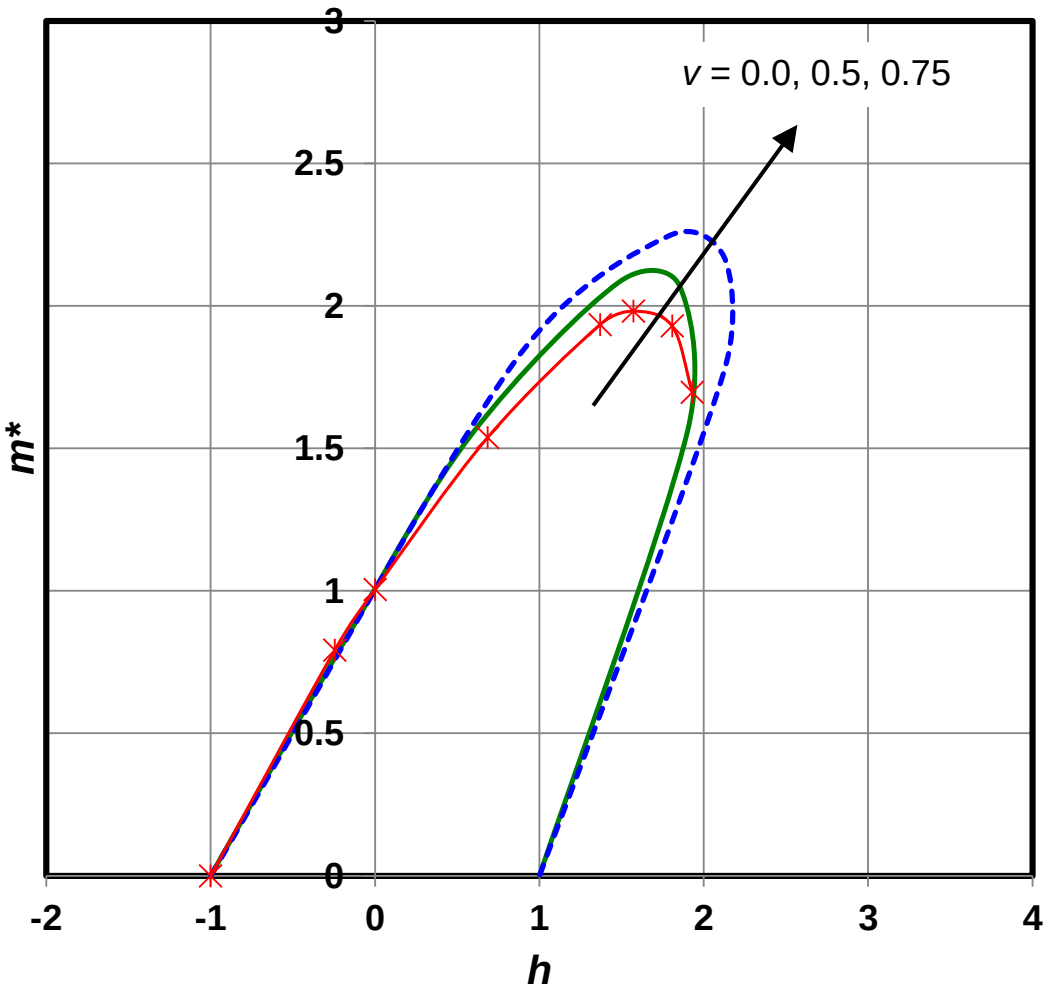

(b) T_s/D = 0.4

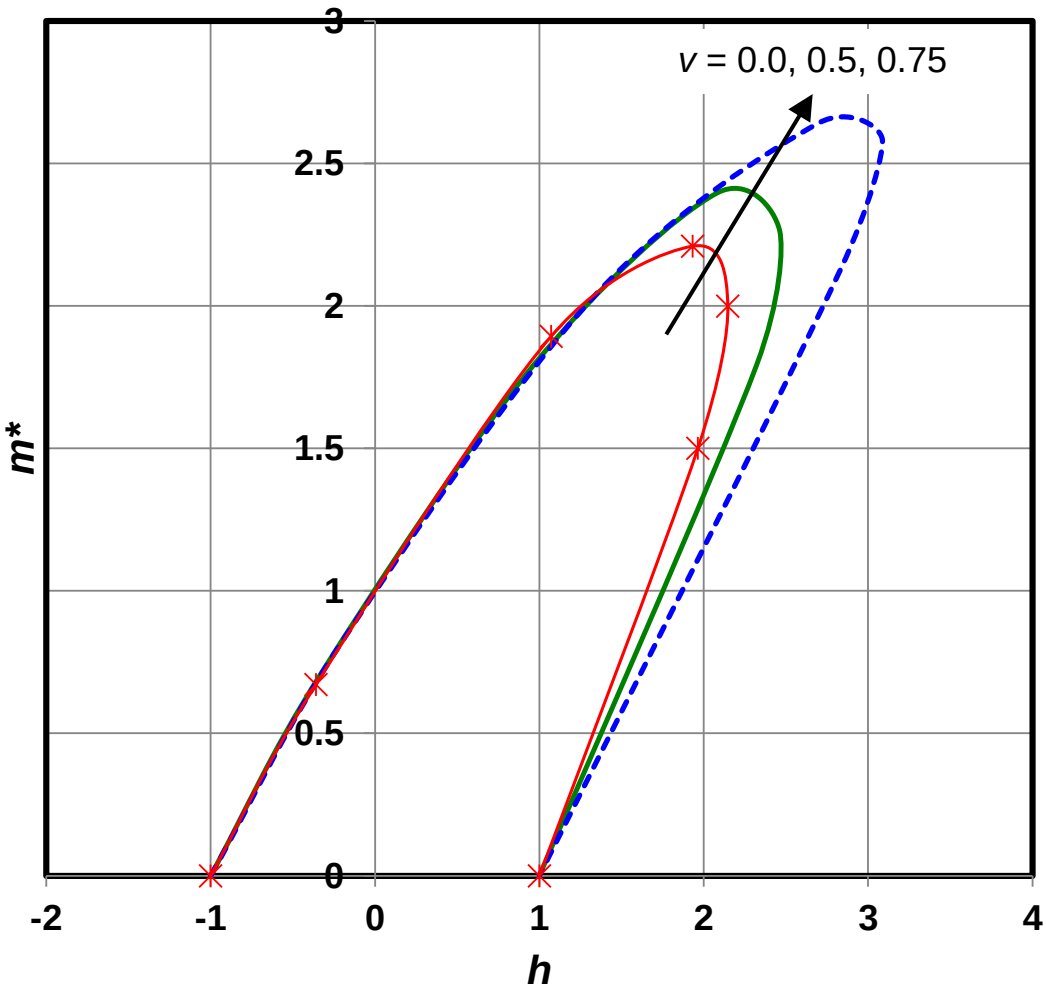

(c) T_s/D = 0.6

Figure 16 Effect of vertical mobilisation *v* on normalised failure envelopes in *h*-*m* space: *d*/*D* = 1.0

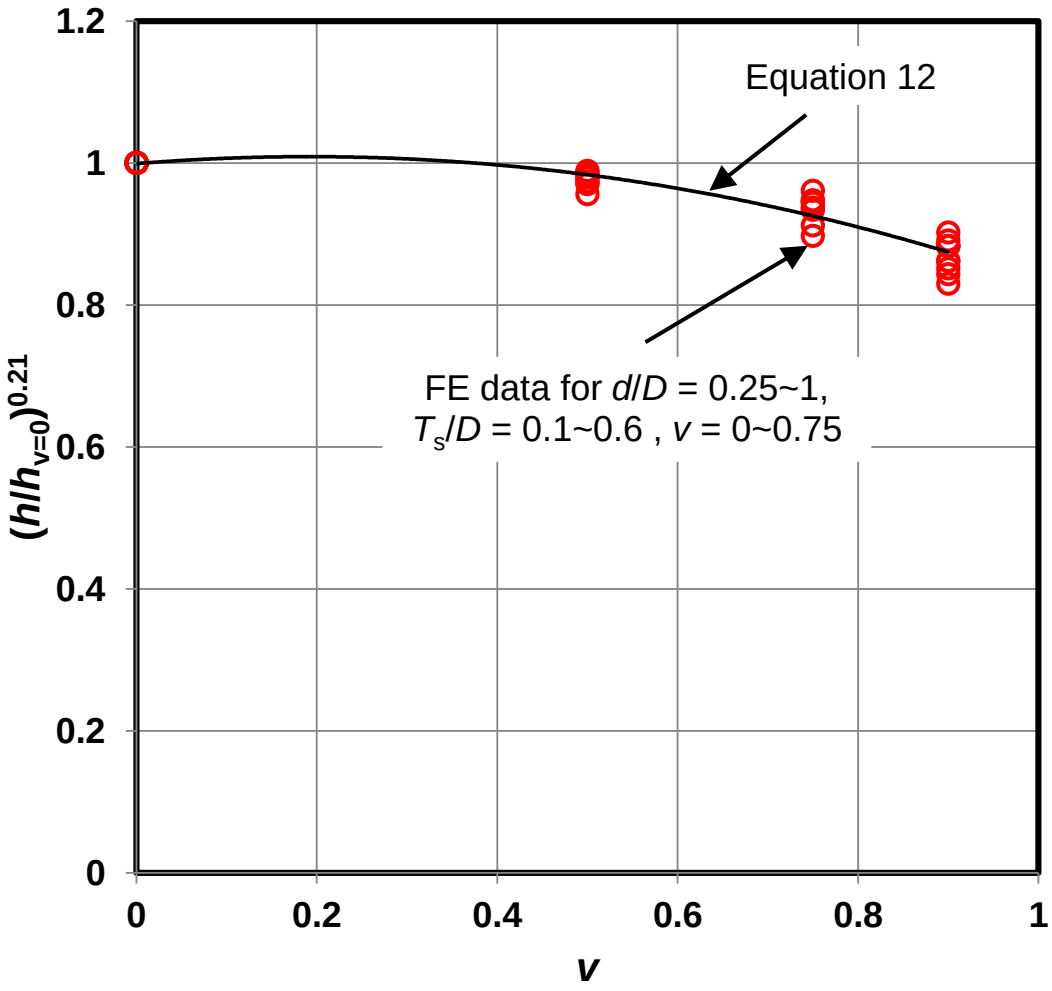

961
962 (a) *v*-*h* space
963
964

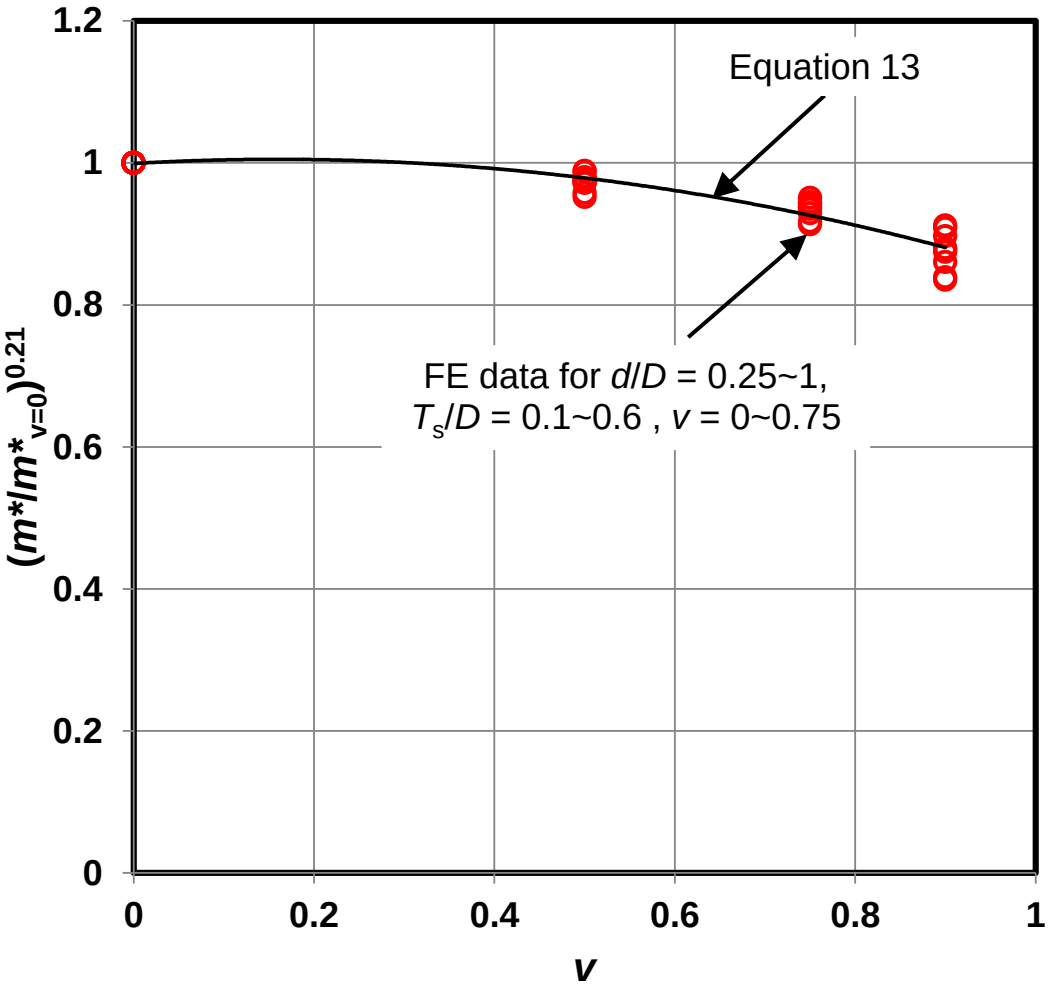

(b) *v*-*m** space

Figure 17 Design charts for quantifying effect of vertical mobilisation *v*